

INTELLIGENT ENERGY MANAGEMENT AGENT
FOR A PARALLEL HYBRID VEHICLE

A Dissertation
by
JONG-SEOB WON

Submitted to the Office of Graduate Studies of
Texas A&M University
in partial fulfillment of the requirements for the degree of
DOCTOR OF PHILOSOPHY

May 2003

Major Subject: Mechanical Engineering

INTELLIGENT ENERGY MANAGEMENT AGENT
FOR A PARALLEL HYBRID VEHICLE

A Dissertation

by

JONG-SEOB WON

Submitted to Texas A&M University
in partial fulfillment of the requirements
for the degree of

DOCTOR OF PHILOSOPHY

Approved as to style and content by:

Reza Langari
(Chair of Committee)

Darbha Swaroop
(Member)

Mehrdad Ehsani
(Member)

Sooyong Lee
(Member)

John Weese
(Head of Department)

May 2003

Major Subject: Mechanical Engineering

ABSTRACT

Intelligent Energy Management Agent for a Parallel Hybrid Vehicle. (May 2003)

Jong-Seob Won, B.S., Pusan National University, Korea;

M.S., Texas A&M University

Chair of Advisory Committee: Dr. Reza Langari

This dissertation proposes an Intelligent Energy Management Agent (IEMA) for parallel hybrid vehicles. A key concept adopted in the development of an IEMA is based on the premise that driving environment would affect fuel consumption and pollutant emissions, as well as the operating modes of the vehicle and the driver behavior do. IEMA incorporates a driving situation identification component whose role is to assess the driving environment, the driving style of the driver, and the operating mode (and trend) of the vehicle using long and short term statistical features of the drive cycle. This information is subsequently used by the torque distribution and charge sustenance components of IEMA to determine the power split strategy, which is shown to lead to improved fuel economy and reduced emissions.

With love,

this dissertation is dedicated to

my parents who are my eternal home of mind,

my gentle, encouraging wife So-Ra,

my adorable son Doo-Hyeon, and

my parents-in-law who presented me with my lovely wife.

ACKNOWLEDGMENTS

This dissertation has come about as the result of a few good ideas and a lot of hard work, but like everything accomplished in life, was possible only with the help and support of others, and gifts and blessings for which I can never take credit. In these acknowledgements, I hope to express a measure of my gratitude to some of those who have had the most profound impact in making this accomplishment possible.

First, I thank my advisor Reza Langari, who opened my eyes to this area of research, for his guidance and support throughout the work leading to this dissertation. It is impossible to sufficiently express my gratitude to him for taking me as his student and sharing with me his vast wealth of engineering knowledge. I thank him for all he has taught me.

I would like to thank Dr. Darbha Swaroop, Dr. Sooyong Lee, and Dr. Mehrdad Ehsani for serving as members on the advisory committee and for providing suggestions and corrections to this dissertation.

I am truly grateful to many people who have given me practical support, shared their knowledge with me and encouraged me. I have a special debt of gratitude to Dr. Yimin Gao and Dr. Hassan Moghbelli, who shared their valuable knowledge with me and took time for invaluable discussion. I thank my fellow students here at Texas A&M, without whom I never could have made it through the Ph.D program.

On a personal note, I first thank my parents, who have given me boundless support in my life. Their steady love, encouragement, and support have sustained me in my growing up years, and even still do today. Thanks again for being there when I needed you. I am thankful to be blessed with parents-in-laws, Jeong-Ho Ahn and Gui-Ryei Bang, who also have been tremendously supportive and encouraging to me throughout my studies.

I also thank my son Doo-Hyeon, who has brought great joy in my life, and whose birth provided me some extra motivation to finish my dissertation. Finally, of all people, I am most thankful for my wife, So-Ra, who has been by far the greatest blessing to me in my life. Without her love and companionship, I don't see how I

could have accomplished this goal.

TABLE OF CONTENTS

CHAPTER		Page
I	INTRODUCTION	1
	1.1 Energy Management in Hybrid Electric Vehicles	1
	1.2 Key Issues and Literature Search	1
	1.3 Contribution of the Dissertation	2
	1.4 Organization of the Dissertation	3
II	ENERGY MANAGEMENT IN HYBRID ELECTRIC VEHICLE	5
	2.1 Hybrid Electric Vehicle Configuration	5
	2.1.1 Series Hybrid Configuration	7
	2.1.2 Parallel Hybrid Configuration	7
	2.1.3 Series-Parallel Hybrid Configuration	8
	2.2 Energy Management Issues	8
	2.3 Existing Approaches	9
	2.3.1 Classical and Fuzzy Logic Based Approach	9
	2.3.2 Optimization Based Approach	11
	2.4 Conclusion	12
III	INTELLIGENT ENERGY MANAGEMENT AGENT	13
	3.1 Introduction	13
	3.2 IEMA Architecture	13
	3.3 Drive Cycle Analysis	15
	3.3.1 Driving Information Extractor (DIE)	15
	3.3.2 Driving Situation Identifier (DSII)	16
	3.3.2.1 Roadway Type Identifier (RTI)	16
	3.3.2.2 Driving Trend Identifier (DTI)	27
	3.3.2.3 Driving Mode Identifier (DMI)	28
	3.3.2.4 Driver Style Identifier (DSI)	29
	3.4 Intelligent Energy Management Strategies	33
	3.4.1 Fuzzy Torque Distributor (FTD)	33
	3.4.1.1 Overview	33
	3.4.1.2 Preliminary Concepts for Rule Base Design	34
	3.4.1.3 Low Speed Cruise Trend	36
	3.4.1.4 High Speed Cruise Trend	36

CHAPTER	Page
3.4.1.5 Acceleration/deceleration Trend	40
3.4.2 Drive Style Compensation	47
3.4.3 SOC Compensator (SCC)	48
3.4.3.1 Battery Charge Operation	48
3.4.3.2 Charge Sustaining Strategy in Hybrid Mode	49
3.4.3.3 Charge Sustaining Strategy in Stop Mode	52
3.4.3.4 Vehicle Mode-Based Charge Operation in Hybrid Mode	57
3.5 Conclusion	58
IV SIMULATION STUDY	60
4.1 Hybrid Vehicle Configuration	60
4.2 Simulation Factors Affecting Performance of IEMA	60
4.3 Evaluation on the Facility-Specific Drive Cycles	62
4.3.1 Effect of Roadway Type Identifier (RTI)	63
4.3.1.1 Effect of RTI under [DSI,DTI]=[OFF,OFF]	64
4.3.1.2 Effect of RTI under [DSI,DTI]=[ON,ON]	64
4.3.2 Effect of [DSI,DTI] under RTI=[ON]/[OFF]	66
4.3.3 Effect of [DSI,DTI] versus RTI	66
4.3.4 Overall Effect of Subsystems	71
4.4 Evaluation on the Urban Dynamometer Driving Schedule	71
4.4.1 Effect of Subsystems	71
4.4.1.1 Effect of RTI	73
4.4.1.2 Effect of [DSI,DTI]	75
4.4.2 Effect of Initial Roadway Type	75
4.4.2.1 RTI=[OFF]	76
4.4.2.2 RTI=[ON]	76
4.4.3 Effect of Time Setting	79
4.4.4 Comments on Roadway Type Identification	82
4.5 Conclusions	82
V CONCLUSION	85
REFERENCES	87
APPENDIX A	91
VITA	93

LIST OF TABLES

TABLE	Page
3.1 Driving pattern factors and their characteristic parameters	17
3.2 Facility-specific drive cycles	18
3.3 Parameter transformation into array	22
3.4 Summary of statistics of facility-specific drive cycles with total journey (See Appendix A)	23
3.5 LVQ network result: MSE of the network, 0.0162; Size of S^1 , 110 (= 2×55)	26
3.6 Description of driving trend	27
3.7 Description of driving mode	29
3.8 Representation of driving style with acceleration and standard deviation	31
3.9 Rule set for fuzzy DSI	32
3.10 Rule base of the FTD: low-speed cruise trend	39
3.11 Rule base of the FTD: high-speed cruise trend	41
3.12 Rule base of the FTD: acceleration/deceleration trend	46
3.13 Sectional division of the engine-motor torque plane	51
3.14 Rule set for mode-based charge operation in the hybrid mode	58

LIST OF FIGURES

FIGURE	Page
2.1 Typical HEV configurations	6
3.1 Intelligent energy management agent architecture	15
3.2 Facility-specific drive cycles	20
3.3 Architecture of the LVQ network	21
3.4 Validation of trained LVQ network on the freeway, LOS E drive cycle (Class 4)	24
3.5 Training data generation: subclass and its class	25
3.6 Membership functions in DTI	28
3.7 Membership functions in DMI	30
3.8 Membership functions in DSI	32
3.9 Structure of FTD rule base	34
3.10 Membership functions in FTD	35
3.11 Fuel consumption rate as function of average speed for passenger car (Vehicle operating speed range $[v_{avg} - v_{std}, v_{avg}, v_{avg} + v_{std}]$ for facility- specific drive cycles)	37
3.12 Representative factors affecting emissions and fuel consumption in each facility-specific drive cycle	38
3.13 Illustration of charge sustaining operation	50
3.14 Definition of torque margins on the engine-motor torque plane	53
3.15 Saturation function for charge sustaining operation	54
3.16 Representation of torque balance constraint in the stop mode	55
3.17 Membership function of output variable in mode-based charge operation	59
4.1 Parallel hybrid drivetrain configuration	61
4.2 Simulation factors	62

FIGURE	Page
4.3 Effect of RTI under [DSI,DTI]=[OFF,OFF]	65
4.4 Effect of RTI under [DSI,DTI]=[ON,ON]	67
4.5 Effect of [DSI,DTI] under RTI=[OFF]	68
4.6 Effect of [DSI,DTI] under RTI=[ON]	69
4.7 Effect of [DSI,DTI] versus RTI	70
4.8 Overall effect of subsystems	72
4.9 EPA Urban dynamometer driving schedule	73
4.10 Decomposition of UDDS through roadway type identification	74
4.11 Effect of IRT when RTI is off; $T_{st} = 10$ sec (for $T_{iu}=10$ sec)	77
4.12 Effect of IRT when RTI is off; $T_{st} = 15$ sec (for $T_{iu}=10$ sec)	78
4.13 Effect of IRT when RTI is on; $T_{st} = 10$ sec (for $T_{iu}=10$ sec)	80
4.14 Effect of IRT when RTI is on; $T_{st} = 15$ sec (for $T_{iu}=10$ sec)	81
4.15 Performance results on the UDDS: $[T_{lt}, T_{st}, T_{iu}] = [150, 10, 10]$ sec; IRT = RT9; [DSI,RTI,DTI] = [ON,ON,ON]	83

CHAPTER I

INTRODUCTION

1.1 Energy Management in Hybrid Electric Vehicles

Hybrid electric vehicles (HEVs) have great potential as new alternative means of transportation. The specific benefits of HEVs, compared to conventional vehicles, include improved fuel economy and reduced emissions [1]-[3]. On the other hand, design and implementation of HEVs present a number of challenging problems. In particular, management of energy and distribution of torque (power) are two of the key issues in the development of hybrid electric vehicles [4]-[28]. These issues can be summarily stated as follows:

- How to meet the driver's torque demand while achieving satisfactory fuel consumption and emissions.
- How to maintain the battery state of charge (SOC) at a satisfactory level to enable effective delivery of torque to the vehicle over a wide range of driving situations.

1.2 Key Issues and Literature Search

As stated in the introductory remarks, a number of studies on energy management for hybrid electric vehicles have been performed in the past. In particular, at least three *logic* based control strategies for distributing power demand have been suggested in [4]-[6]. Likewise, fuzzy logic based energy management strategies are proposed in

The format and style follow that of *IEEE Transactions on Intelligent Transportation Systems*.

several studies [7]-[15]. These approaches are adopted mainly because of their effectiveness in dealing with problems appearing in the complexity of hybrid drivetrain via both heuristics (and human expertise) and mathematical models. However, these approaches generally do not address the driving situation that may affect the operation of the vehicle.

The application of optimal control theory to power distribution for hybrid vehicles appears promising as well, as noted in [16]-[18]. In addition, a number of studies, dating back to 1980s, have focused on the application of dynamic programming to HEVs [19]-[21]. These and the aforementioned optimal control strategies are, however, generally based on a *fixed* drive cycle, and as such do not deal with variabilities in driving situations. In view of this issue a number of alternative optimization approaches have been proposed in the literature [22]-[27]. In particular, [28] formulated a drive cycle dependent optimization approach that selects the optimal power split ratio between the motor and the engine according to the characteristic features of the drive cycle.

In general, however, few, if any, of the aforementioned studies have given appropriate consideration to driving situations and/or the driving style of the driver.

1.3 Contribution of the Dissertation

This dissertation deals with a conceptual design of new intelligent energy management system applicable to parallel HEVs. This design was motivated by some limitations of existing approaches for energy management control (addressed in detail in Chapter II), whose main stream focused on single-layered approaches that use only the *current* vehicle state for decision-making in connection with torque distribution and charge sustenance tasks; little consideration is generally given to driving situations and driving style of the driver [28]. As a result, the majority of the proposed concepts do not address the effects of variations in driving situations on the vehicle emissions and fuel consumption over the spectrum of driving situations to which the vehicle may be subjected.

In this dissertation, a “driving situation awareness”-driven intelligent energy management system for parallel HEVs is proposed and developed. A key concept adopted in the development of an energy management system is based on the idea that driving environment (situation) as well as the driving modes of operation of the vehicle and the driving style of the driver directly affect fuel consumption and pollutant emissions. To implement this idea, an intelligent energy management system has been designed, which has integrated functioning for dealing with information about driving situation, driving style, and driving mode of operation of the vehicle and for performing energy management task in connection with torque distribution and charge sustenance. The proposed system includes the design of a number of subsystems each of which has its own mission: (1) Driving Information Extractor (DIE); (2) Driving Situation Identifier (DSII) consisted of Roadway Type Identifier (RTI), Driving Style Identifier (DSI); (3) Fuzzy Torque Distributor (FTD); (4) State-of-Charge Compensator (SCC).

The main contributions in this dissertation are, through the design of proposed energy management system, to describe the underlying framework for implementation of each of these components (subsystems) and the manner in which they function together to address the problem of energy management and torque distribution in HEVs. The following summary provides the additional aspect of the proposed design:

- Systematic methodology: This design proposes a systematic way to consider the driving situation in the design of energy management system for HEVs.
- Modular design: Through the modular designs of the subsystems, it enables the subsystems to be applicable to other uses.
- Performance improvement: Simulation results reports that the overall performance is improved under the direction of the proposed IEMA, which shows its viability for energy management system of parallel hybrid vehicles.

1.4 Organization of the Dissertation

Following this introduction, Chapter II provides a general description of energy management issues in the operation of hybrid electric vehicles. Three typical hybrid

configurations - series, parallel, and series-parallel hybrid - are enumerated and illustrated. More detailed descriptions of existing approaches for energy management in HEVs are given. Furthermore, the limitations of existing approaches are also discussed.

Chapter III presents the development of a “driving situation awareness”-driven intelligent energy management agent (IEMA). The key concept of the proposed energy management system is illustrated. The proposed concept incorporates several subsystems each of which has its own mission. Details of design methodologies of subsystems are described. Again, this chapter describes the underlying framework for the implementation of each of these subsystems and the manner in which they function together to address the problem of energy management of a parallel HEV.

The implementation of IEMA and the simulation work for the validation of IEMA are performed in Chapter IV. Evaluation of proposed energy management system are made through computational simulation works on a set of nine facility-specific drive cycles and the Urban Dynamometer Driving Schedule (UDDS). Simulation results are analyzed and reported to show its viability for energy management of a parallel HEV.

Finally, concluding remarks of this dissertation are summarized in Chapter V.

CHAPTER II

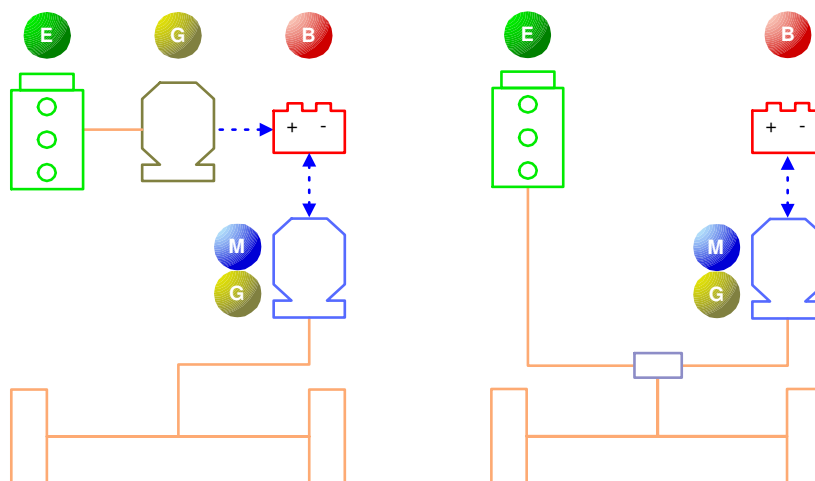
ENERGY MANAGEMENT IN HYBRID ELECTRIC VEHICLE

2.1 Hybrid Electric Vehicle Configuration

The general definition of HEVs, although available in many ways, is that an HEV is a vehicle in which propulsion energy is available from two or more kinds of energy sources, or converters, and at least one of them can deliver electric energy. Candidates for energy sources can be a spark-ignited or diesel engine, a turbine or perhaps a fuel cell and an electric motor. As an electric energy storage device, a battery, flywheel or ultracapacitor can be equipped and utilized.

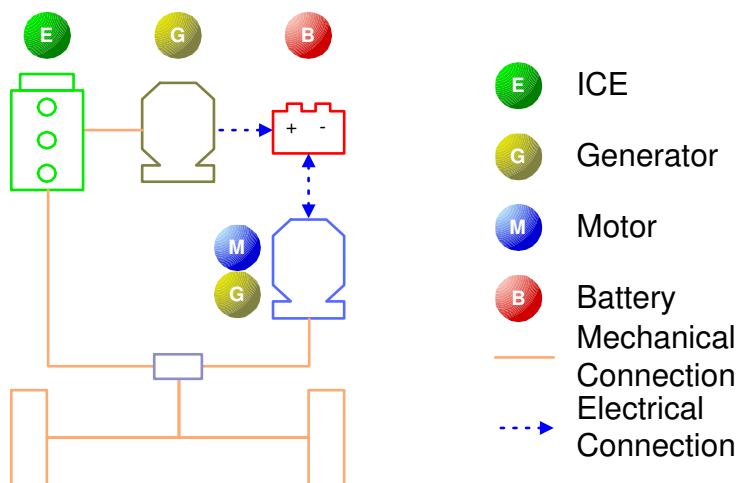
The propulsion system (powertrain) in a vehicle can be defined as the components generating or transforming power necessary for propulsion. Depending on the ways the components can be chosen and arranged, hybrid powertrains, which in the case of hybrid electric vehicles (HEVs), can be classified into several categories. Typically, HEVs are classified into two basic categories - serial and parallel (See Fig. 2.1.) The main difference in the two powertrain configurations is the connection of power components with the wheels. By taking beneficial features of both configurations, a series-parallel hybrid is added to the list of classifications.

In the series hybrid, the internal combustion engine (ICE) is coupled with the generator to produce the electricity and no connection is made between the ICE and the wheels, resulting in a pure electric propulsion. In the parallel hybrid, both the ICE and the electric motor (EM) are coupled with the wheels for propelling the vehicle. In the series-parallel hybrid, there are several possible ways to operate the vehicle for different driving conditions.



(a) Series hybrid

(b) Parallel hybrid



(c) Series-Parallel hybrid

Figure 2.1 Typical HEV configurations

2.1.1 Series Hybrid Configuration

In the series hybrid, there is no mechanical connection between the ICE and the wheels. Only the electric motor drives the wheels and the engine is used to generate electricity (through a generator) for charging the battery. The electricity from the generator can be used either to charge the battery or to provide the propulsive power to the wheels through the motor. Due to the decoupling between the ICE and the wheels, the ICE can be operated in its efficient operating region, while maximizing fuel efficiency for generating electricity. While this configuration is simple, there are two issues that must be considered in this design - efficiency and cost: (1) The energy conversion (transformation) losses among components (from the ICE through the generator, the battery, and the motor to the wheels in the form of chemical energy through mechanical energy and electrical energy to mechanical energy) deteriorates the efficiency of the series drivetrain; (2) Components sizing to cover high power demand, such as in heavy acceleration or uphill climbing, causes the series hybrid to be expensive.

2.1.2 Parallel Hybrid Configuration

Direct delivery of propulsion power from both energy sources to the wheels is available in the parallel hybrid due to the (mechanical) coupling of both the ICE and the motor to the wheels. In the parallel hybrid, the ICE, the motor, or both power sources can be utilized to provide power to the wheels. The ICE can power the vehicle and recharge the battery using the motor as a generator. For instance, one portion of the engine power directly drives the wheels and the rest of the power goes through the electric path if surplus power from the engine is available. The regeneration of electric energy during braking is accomplished in the motor (functioning as a generator) that would otherwise be wasted, as in a series hybrid.

The main advantages of the parallel hybrid over the series hybrid are in: (1) its energy conversion efficiency due to the mechanical connection between the ICE and the wheels, reducing the amount of power conversion from energy sources; (2) the

downsized engine (and motor) due to its co-assisted capability in terms of propulsion power generation, resulting in enhanced fuel economy and reduced pollutant emissions.

2.1.3 Series-Parallel Hybrid Configuration

The series-parallel hybrid is, as the name suggests, a combination of a series and parallel hybrid. In this type of hybrid, there are several possible ways to operate the vehicle - series, parallel, even some combination of both - for different loading conditions. This would utilize the advantages of both types of drivetrain. Depending on the driving situations, the most advantageous mode could be selected. This topology would, however, suffer from a more complicated structure and higher cost than either a series or a parallel does.

2.2 Energy Management Issues

The gains in fuel economy associated with the introduction of HEVs is promising for the automotive industry. However, in order to realize these gains major challenges in HEV design and operation, such as coordinating (managing) multiple energy sources, which is highly dependent on the configuration of drivetrain, components sizing, and other factors that affect the operation of HEVs, must be overcome.

The overall performance of an HEV with respect to fuel economy and emissions reduction is dependent not only on how the individual components are efficiently designed but also on how the operation of components is coordinated with each other. That is, to maximize the advantages of hybrid drive, the following consideration should be made in parallel both in the design phase and in the operation phase of an HEV [29]: enhancement of powertrain components efficiency; optimal design of hybrid powertrain system; energy management control system design. In this dissertation, I concentrate on the development of energy management system for a parallel HEV. Energy management strategy in HEV operation, especially, the coordination of energy

flow in the powertrain, consists of two basic tasks: Torque distribution (torque split) task and charge sustenance task. The first task refers to the decision-making on the use of energy sources under a driving situation, while meeting driver's torque demand. The second task reflects the extended driving capability of HEVs through controlling the operation of the battery. These two are the main issues in the development of energy management system coordinating the functioning of the energy sources and the energy flow in the hybrid powertrain.

2.3 Existing Approaches

A number of control strategies to cope with these issues have been presented in literature. This section provides a brief review of existing work being performed in the area of energy management control for hybrid electric vehicles.

2.3.1 Classical and Fuzzy Logic Based Approach

Researches on classical and/or fuzzy logic based approach for energy management strategy of hybrid vehicles have been performed in the following literature:

Few strategies for *logic* based approach are available in literature [4]-[6]. Buntin et al. in [4] designed a logic based switching control system for a parallel HEV with the objective of achieving acceptable vehicle performance and maximizing the state of charge of the battery throughout driving. To achieve this objective, control regions and control logic making pairs with each region are defined on the torque-speed plane. According to the driver torque demand, a control scheme under the control region is activated to meet driver torque demand while maximizing the battery state of charge.

Jalil et al. in [5] presented a rule based control and energy management strategy for a series HEV. Their strategy aims at a power split (assignment) in a way that both power sources - engine and battery - are operated at high efficiency. The idea of power split was implemented under a rule-based frame that controls power assignment based on the status of the SOC, the power demand, and the acceleration command.

Liang et al. in [6] presented a logic based control strategy for a parallel HEV focusing on the best SOC (for acquiring maximum vehicle driving range.) For each vehicle modes - propelling and braking, engine and motor power are determined by the control logics which are set based on the operation modes of the engine and the motor given driver power demand.

Again, fuzzy logic based control strategies for hybrid vehicles are available in literature [7], [8], and [11]-[15]. Cerruto et al. in [7] and [8] presented a fuzzy logic based power regulator to the control of power flow in a (series) hybrid HEV.

Koo et al. [11] proposed a fuzzy logic torque controller for a parallel HEV with the control objectives of improving driveability, balancing of battery charge, and reducing NOx (nitrogen oxide) emissions. To realize this, the construction of fuzzy rule bases was performed based on the dynamo test of parallel driving system. The proposed fuzzy controller has two units, each of which has its own fuzzy rule base, one is for driver's intention predictor (based on acceleration and its rate) and the other for power balance controller (based on the engine speed and vehicle speed.)

Won et al. [14] presented a vehicle operating mode-based fuzzy torque distribution control for a parallel HEV. The proposed controller is implemented in terms of a hierarchical architecture which incorporates the modes of operation of the vehicle as well as empirical knowledge of energy flow in each mode. Moreover, the rule set for each mode of operation of the vehicle is designed in view of an overall energy management strategy that ranges from maximum emphasis on battery charge sustenance to complete reliance on the electric power source.

In [13] and [15], the authors developed a power controller for a parallel HEV that will optimize the fuel economy by demanding all major power components - the engine, the motor, and the battery - to operate at each efficient region of operation of each component. The implementation was made via fuzzy logic control, which provides a method for realizing an optimal trade-off between the efficiencies of all components.

Similarly, in [12], Brahma et al. designed fuzzy logic, rule-based controller to optimize the energy efficiency through the control of the power flows of a parallel HEV by commanding the engine to operate at its efficient operating region.

2.3.2 Optimization Based Approach

Some existing research works in the optimization based approach are available for scrutiny in [22]-[24], and [26]-[28]. In general, the solution to the optimal torque distribution (power split) problem is ultimately dependent on the objective (cost) defined. Fuel efficiency optimization problem with the energy-based cost function is shown in [22] and [27]. In [22], the aim of the control optimization is to minimize the energy-based objective function with torque split and gear ratio as the control variables. Especially in [27], a multi-objective nonlinear optimal torque distribution strategy is formulated and converted into a single-objective linear programming problem by linearization of the objective functions and by introducing an equivalent energy consumption rate for the fuel flow rate. In [26], by introducing the equivalent fuel flow rate for the use of the electric machine, an instantaneous optimization problem with the objective of equivalent fuel flow rate for power split is formulated and solved. Again the same formulation is extended to enforce emission reduction with the appropriate weighting coefficients which penalty equivalent fuel flow rates in the objective function. Kim et al., [23] introduced an effective specific fuel consumption that is used as equivalent fuel consumption in the electric drive in which battery output power is transformed into an equivalent amount of fuel for finding optimal torque distribution solution in the parallel HEV operation. The application of convex optimization to the problem of finding optimal engine operation in a series hybrid vehicle over a fixed drive cycle is addressed in [24].

Dynamic programming approach for the development of hybrid vehicle control strategy can also be found in the literature. In [19] and [20], aim was to optimizing the energy transfer and conversion in the hybrid powertrain by dynamic programming using criterion of minimization of fuel consumption within a given drive cycle. Also, Brahma et al. [21] formulated the optimal power split problem for series hybrids and solved the problem using a dynamic programming approach.

Optimization technique with driving pattern recognition is also addressed in [28]. In particular, the authors of [28] considered six representative drive cycles and found optimal control parameters being used in the objective function to find optimal power

split ratio. During the operation of the vehicle, the study proposed to find optimal power split ratio using control parameters that forms a pair with the recognized drive cycle. However, optimized control action, due to its dependency on a specific drive cycle used in optimization process, may not be an optimal one for a misclassified drive cycle, or an arbitrary drive cycle segment which seems not to be a part of drive cycles used in the generation of optimal control action.

2.4 Conclusion

It is evident that most of methodologies used in literature provide solutions to the problem of energy management control in HEV operation. Their control strategies, however, are based on the consideration of the *current* vehicle state, e.g., State-of-Charge (SOC), vehicle speed, engine speed, motor speed, given driver demand, although real driving occurs under a driving environment that would affect vehicle operation, consequently fuel consumption and pollutant emissions. Little consideration is given in the development of an energy management system to the effect of modal transition of the vehicle and driving situation that would affect the driving pattern of the vehicle and the driving style of the driver.

It is understood that the following two considerations would be a guide to cope with the limitation of existing approaches: First, since, in my view, the aforementioned approaches do not adequately reflect the reality of the operation of hybrid vehicles, which must perform well across a spectrum of operating regimes, a driving mode and trend (modal transition)-based energy management strategy is suggested to overcome the shortcomings of the aforementioned approaches. Second, it is suggested that the design of a system architecture be accomplished, which can address the problem of driving situation awareness within the overall energy management strategy.

CHAPTER III

INTELLIGENT ENERGY MANAGEMENT AGENT

3.1 Introduction

In this chapter, a novel architecture for energy management system of parallel hybrid electric vehicles is proposed - Intelligent Energy Management Agent (IEMA). This architecture incorporates a concept of *driving situation awareness* in an energy management system with traditional missions of torque distribution and charge sustenance operation. The key element of this architecture is the identification of the driving situation of the vehicle. The driving situation assessment is realized by the driving situation identification components, each of which has its own mission. Design methodologies of components are presented in detail. In connection to driving situation awareness, energy management strategy for power split operation (torque distribution and charge sustenance) are presented.

3.2 IEMA Architecture

The primary function of IEMA is to distribute the required torque between the electric motor and the ICE (Internal Combustion Engine). In order to accomplish this, IEMA utilizes four sub agents - Driving Information Extractor (DIE), Driving Situation Identifier (DSII), Fuzzy Torque Distributor (FTD) and State-of-Charge Compensator (SCC) (See Fig. 3.1.) The function of these components is as follows:

- Driving Information Extractor (DIE): The mission of DIE is to extract the key statistical features, or characteristic parameters, of the driving pattern. These parameters are subsequently used to determine the roadway type, driving style of the driver, driving trend, and generally characterize the driving situations.

- Driving Situation Identifier (DSII): The overall traffic environment, including the vehicle's operating mode, is identified by the driving situation identifier (DSII). DSII incorporate the following components:
 - Roadway Type Identifier (RTI)
 - Driver Style Identifier (DSI)
 - Driving Trend Identifier (DTI)
 - Driving Mode Identifier (DMI)

While details of each of these components is described in a later section, it should be noted that DSII relies extensively on the Driving Information Extractor (DIE) to perform its function.

- Fuzzy Torque Distributor (FTD): The function of FTD is to determine the effective distribution of torque between the motor and the engine. The key relationship involved is as follows:

$$T_e + \underbrace{\overbrace{T_{ec,FTD}}^{\text{propulsion}} + \overbrace{T_{ec,SOC}}^{\text{charging}}}_{\text{Engine}} + \underbrace{T_{mc}}_{\text{Motor}} = T_c \quad (3.1)$$

where T_c is the driver's torque demand; T_e is the current engine torque; $T_{ec,FTD}$ and $T_{ec,SOC}$ are the increment of engine torque for propulsion and charging the battery, respectively; T_{mc} is the motor torque command which together with the engine torque command ($T_e + T_{ec,FTD} + T_{ec,SOC}$) meets the driver's torque demand.

- State of Charge Compensator (SCC): In principle, the commanded output for the HEV operation from the torque distribution operation cannot guarantee the sustenance of the charge of the battery over the unknown range of driving to which the vehicle may be subject. To add the capability of extension of driving range, it should be guaranteed that the level of electric energy available through the electric energy storage is maintained within a prescribed range throughout driving. In this study, a state-of-charge compensator (SCC) is proposed and incorporated into IEMA to achieve the goal of the charge-sustenance task.

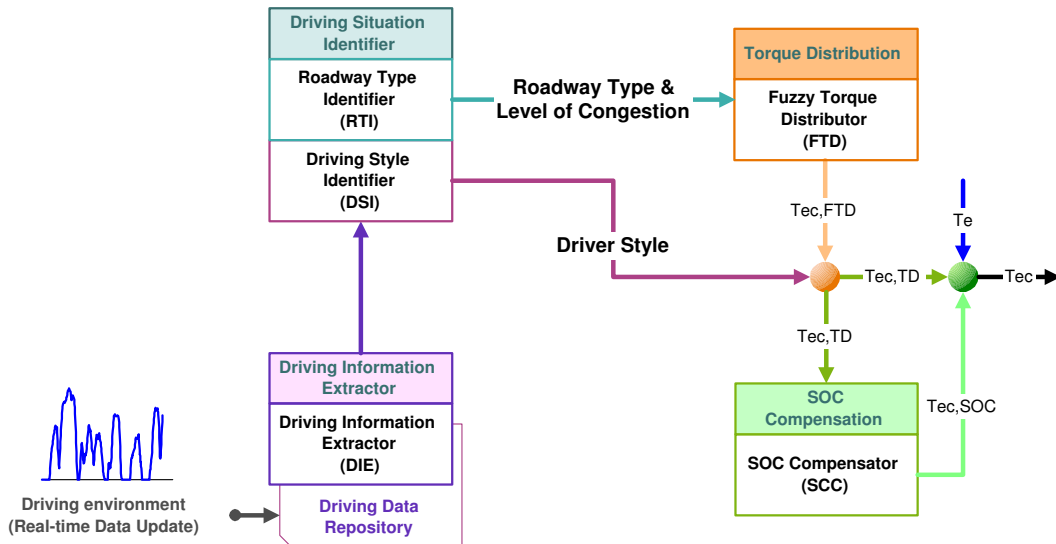


Figure 3.1 Intelligent energy management agent architecture

3.3 Drive Cycle Analysis

A key feature of IEMA is its ability to use drive cycle analysis to determine the characteristics of the driving pattern. The two components that perform the function are Driving Information Extractor (DIE) and the Driving Situation Identifier (DSII). These two components are discussed below.

3.3.1 Driving Information Extractor (DIE)

Driving pattern (history) in real driving is the product of the instantaneous decisions of the driver to cope with the (physical) driving environment. Driving pattern is generally defined in terms of the speed profile of the vehicle in a particular environment [30]. The mission of DIE is to extract the key statistical features, or *characteristics parameters*, of the driving pattern. While there is no consensus among researchers as to the precise definition of these parameters, a number of studies have attempted to define a list of such parameters [28]-[34]. For example, according to

Ericsson [31] up to 62 characteristic parameters may be extracted from a given drive cycle, which she has further divided into 16 groups or factors. Moreover, as pointed out in [31] and [32], 9 out of these 16 factors critically affect fuel-usage and emissions. In Table 3.1, the complete set of 16 driving pattern factors considered by Ericsson are listed and the aforementioned 9 factors are marked by †.

Note that the numeric values shown above are based on the studies performed in Sweden and thus may not be directly applicable to U.S. or Asian driving situations. However, the general theme of the above list of factors is still useful as the basis for developing a driving situation based energy management system. Furthermore, note that it is not generally possible to extract the complete set of 62 parameters suggested by Ericsson [31] from typical drive cycle information. Hence the study reported in this dissertation makes use of 40 such parameters augmented by an additional set of 7 parameters as discussed shortly (See Appendix A.)

3.3.2 Driving Situation Identifier (DSII)

The overall traffic environment including the vehicle's operating mode is identified in the driving situation identifier (DSII). DSII incorporates the following components:

- Roadway Type Identifier (RTI)
- Driver Style Identifier (DSI)
- Driving Trend Identifier (DTI)
- Driving Mode Identifier (DMI)

3.3.2.1 Roadway Type Identifier (RTI)

The mission of RTI is to classify the current traffic situation in terms of roadway types combined with traffic congestion level. Information from RTI is one of several inputs to the fuzzy torque distributor, which will be discussed in later sections. RTI makes use of a learning vector quantization (LVQ) network to classify the current roadway type and congestion level. Before I describe this framework, I need to consider the notion of facility-specific drive cycle.

Table 3.1 Driving pattern factors and their characteristic parameters

Factor	Description (Typical parameter)
1	Deceleration factor (Average deceleration)
2	Factor for acceleration with strong power demand [†] (Relative Positive Acceleration)
3	Stop factor [†] (% of time $v < 2$ km/h)
4	Speed oscillation factor [†] (Frequency of oscillation of the speed curve per 100 sec)
5	Factor for acceleration with moderate power demand [†] (% of time when va is 3-6 m ² /s ³)
6	Extreme acceleration factor [†] (% of time when a exceeds 2.5 m/s ²)
7	Low speed factor (15 ~ 30 km/h*) (% of time when v is 15-30 km/h)
8	High speed factor (90 ~ 110 km/h*) (% of time when v is 90-110 km/h)
9	Mid-high speed factor (70 ~ 90 km/h*) (% of time when v is 70-90 km/h)
10	Mid speed factor (50 ~ 70 km/h*) [†] (% of time when v is 50-70 km/h)
11	Factor for late gear changing from gears 2 and 3 [†] (% of time engine speed is 2500-3500 when in gear 3)
12	High engine speed factor (> 3500 rpm*) [†] (% of time when engine speed is > 3500)
13	Extreme-high speed factor (> 110 km/h*) (% of time when $v > 110$ km/h)
14	Factor for moderate engine speed in gears 2 and 3 [†] (% of time engine speed is 1500-2500 when in gear 2)
15	Factor for low engine speed in gear 4 (% of time engine speed is < 1500 when at gear 4)
16	Factor for low engine speed in gear 5 (% of time engine speed is < 1500 when at gear 5)

Note: The numeric values are from Ericsson [31] based on European standards; v , vehicle speed.

Table 3.2 Facility-specific drive cycles

Facility	Description
1	High-speed freeway
2	Freeway under LOS A-C
3	Freeway under LOS D
4	Freeway under LOS E
5	Freeway under LOS F
6	Freeway under LOS G
7	Freeway ramp
8	Arterial/collector under LOS A-B
9	Arterial/collector under LOS C-D
10	Arterial/collector under LOS E-F
11	Local roadway

Note: See [35] for details in grouping of facility and LOS.

Facility-specific drive cycles. In urban areas, a vehicle can be driven on the road comprising different types of roadways (e.g., local roadway, arterial/collector, and freeway.) Under contract with the Environmental Protection Agency (EPA), Sierra Research Inc. [35] has developed a set of 11 drive cycles that represent passenger car and light truck operations over a range of facilities and congestion levels in urban areas; i.e. Level of Service (LOS.) Note that Level of Service (LOS) [36] is defined as “a qualitative measure describing operational conditions within a traffic stream, based on service measures such as speed and travel time, freedom to maneuver, traffic interruptions, comfort, and convenience. Six types of LOS are defined for each type of facility. These are labeled from A to F, with LOS A representing the best operating conditions and LOS F the worst. Each Level of Service represents a range of operating conditions and the driver’s perception of those conditions; safety is not included in the measures that establish service levels.”

The list of eleven facility-specific drive cycles developed by Sierra Research is shown in Table 3.2.

Based on the definition of LOS, traffic condition with LOS F is categorized as

the most congested situation. Although Sierra created freeway LOS G drive cycle as the worst case of congestion, it can be considered as a subset of freeway LOS F. In addition, the characteristic statistics of the drive cycles show that the freeway ramp cycle seems to be very close to freeway LOS E. With this in mind, only 9 of the 11 facility-specific drive cycles developed by Sierra Research are considered in this study (See Fig. 3.2.¹) These drive cycles are subsequently characterized in terms of their elemental features as defined by Ericsson [31]. The resulting feature vectors constitute the so called training set for a feature based drive cycle classification scheme developed using the so called Learning Vector Quantization (LVQ) methodology. A brief description of this methodology and its usage in the current context is discussed below.

Learning Vector Quantization (LVQ) network. In order to develop RTI, a supervised competitive learning vector quantization (LVQ) network is selected due to its effectiveness in the classification of complex and nonlinearly separable target classes [37]. An LVQ network classifies its input vector into one of a number of target classes through a two stage process. In the first stage, a competitive layer is used to identify the *subclasses* of input vectors. In the second stage, a linear layer is used to combine these subclasses into the appropriate target *classes*. The structure of the LVQ network is shown in Fig. 3.3.

The classification process inside the LVQ network may be briefly described as follows. Each neuron (designated as “**H**”) in the competitive layer of the network computes the Euclidean distance between the given input vector, \mathbf{p} and a prototypical subclass vector \mathbf{w} (template pattern of a specific subclass.) For instance, the *ith* neuron in the competitive layer computes $d = \|\mathbf{w}_i - \mathbf{p}\|$, where $\mathbf{w}_i = [w_{i1} \ w_{i2} \ \dots \ w_{iR}]^T$ and $\mathbf{p} = [p_1 \ p_2 \ \dots \ p_R]^T$ are a prototypical subclass vector and input vector, respectively. Subsequently, the competitive layer (designated as “**C**”) assigns a 1 to the closest subclass to the given input vector and 0 to all other subclasses represented in the network. The linear layer combines the given identified subclasses into a (target)

¹Data courtesy of Carlson and Austin [35].

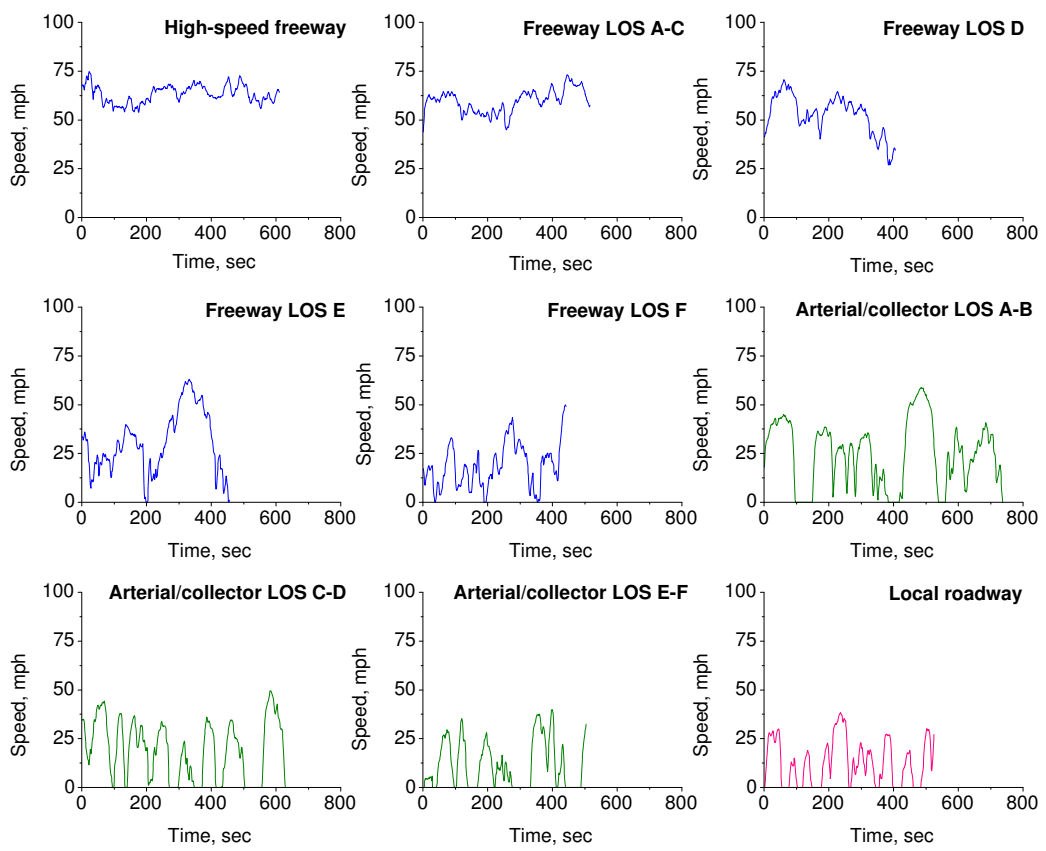


Figure 3.2 Facility-specific drive cycles

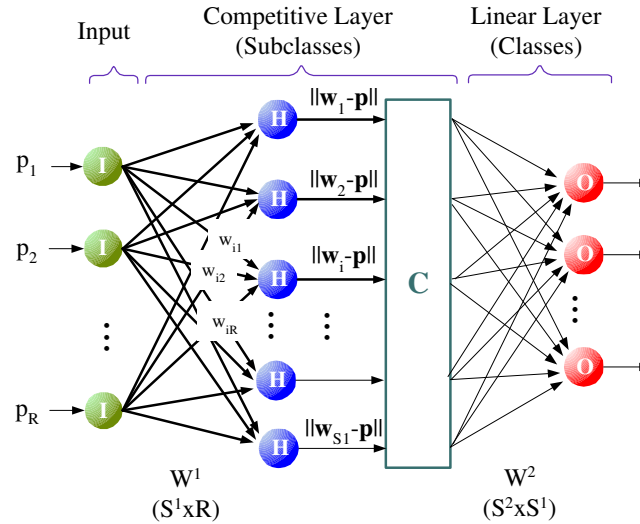


Figure 3.3 Architecture of the LVQ network

class.

Training of the LVQ network. In order to train the LVQ network for roadway type classification, the statistics of nine facility-specific drive cycles [35] were calculated in terms of the characteristic parameters defined in [31] (See Table 3.4.) Note, however, that Ericsson [31] originally defined 62 parameters to describe a driving pattern. In this study, only 40 of the 62 parameters are considered since the information on the engine speed and gear changing behavior is not provided in the drive cycles under consideration. On the other hand, seven other characteristic parameters, which we believe enhance the performance of RTI, are added as follows: trip time; trip distance; maximum speed; maximum acceleration; maximum deceleration; number of stops; idle time, i.e., percent of time at speed 0 km/h (See Appendix A.)

The initial training data set of the LVQ network thus consisted of a $[47 \times 9]$ matrix (See Table 3.4.) In order to enhance the training performance of the network (c.f. convergence to zero of the training error), following [28], each parameter value (p) was transformed into an array with entries of 1 and -1 as described in Table 3.3.

Table 3.3 Parameter transformation into array

Label	Range	Array
L1	$p > p_{avg} + \alpha \times p_{SD}$	[1 1 1]
L2	$p_{avg} < p \leq p_{avg} + \alpha \times p_{SD}$	[1 1 -1]
L3	$p_{avg} - \alpha \times p_{SD} < p \leq p_{avg}$	[1 -1 -1]
L4	$p \leq p_{avg} - \alpha \times p_{SD}$	[-1 -1 -1]

where p_{avg} and p_{SD} are the average and standard deviations, respectively, of a given parameter, p , and α is empirically determined based on the performance of the network. The above process effectively transforms the $[47 \times 9]$ training matrix into a $[141 \times 9]$ matrix but enhances the training performance of the network.

An important factor in the LVQ network is the number of neurons (*subclasses*) (S^1) in the competitive layer. In the particular case at hand, S^1 was set as 9, letting each class be represented by a single subclass.

Validation. The network architecture just described is generally successful in terms of classifying the original set of 9 drive cycles using the 47-parameter feature vectors described earlier. However, this same network did not perform as well on shorter *segments* of these same drive cycles. As an example, consider the Sierra freeway, LOS E drive cycle, (See Fig. 3.4.) While the network properly classifies this drive cycle as belonging to Class 4 when the entire drive cycle is considered, brief segments of this same drive cycle, say from $T = 250 \sim 350$ sec or $T = 300 \sim 400$, were classified as belonging to Class 3, i.e. Sierra freeway, LOS D drive cycle. Similar misclassifications of other segments of the given drive cycle are noted in Fig. 3.4, although it should be emphasized that not every segment is mis-classified.

The reason for the types of mis-classification depicted above was eventually determined to be (1) The use of a single set of characteristic parameters for relatively long drive cycles; (2) The similarity of the statistics of neighboring drive cycles. In

Table 3.4 Summary of statistics of facility-specific drive cycles with total journey (See Appendix A)

Parameters	Units	RT1	RT2	RT3	RT4	RT5	RT6	RT7	RT8	RT9
Trip time	sec	609	515	405	455	441	736	628	503	524
trip distance	km	17.21	13.74	9.58	6.21	3.66	8.15	5.40	2.60	3.01
v_avg	km/h	101.74	95.998	85.075	49.074	29.955	39.828	30.947	18.597	20.67
v_std	km/h	7.24	9.42	15.98	25.43	18.22	26.97	23.95	19.43	18.27
v_max	km/h	120.19	117.62	113.60	101.37	80.29	94.77	79.65	64.20	61.63
a_avg	m/s ²	0.273	0.284	0.311	0.481	0.524	0.557	0.650	0.663	0.589
a_std	m/s ²	0.175	0.201	0.180	0.358	0.417	0.492	0.499	0.500	0.414
a_max	m/s ²	1.207	1.520	1.028	2.369	3.084	2.235	2.548	2.592	1.654
r_avg	m/s ²	-0.279	-0.261	-0.366	-0.580	-0.608	-0.688	-0.714	-0.742	-0.722
r_std	m/s ²	0.191	0.169	0.311	0.617	0.516	0.606	0.616	0.553	0.555
r_max	m/s ²	-1.028	-1.386	-1.743	-3.620	-2.726	-2.950	-3.442	-2.592	-2.637
mm_100m		0.006	0.022	0.052	0.097	0.164	0.061	0.204	0.347	0.167
lmm_100m		0	0	0	0	0	0	0	0	0
mm_100s		0.164	0.583	1.235	1.319	1.361	0.680	1.752	1.789	0.954
lmm_100s		0	0	0	0	0	0	0	0	0
RPA	m/s ²	0.081	0.157	0.163	0.336	0.075	0.196	0.111	1.889	1.904
int_a2	m ² /s ³	24.257	44.067	62.611	149.15	196.88	529	340.61	153.1	523.97
pc_stopt	%	0	0	0	2.418	4.308	15.489	23.089	34.791	27.863
stopdura	sec	0	0	0	11	6.333	28.500	18.125	25.000	20.857
stop_pkm		0	0	0	0.161	0.819	0.491	1.482	2.696	2.327
n_stop		0	0	0	1	3	4	8	7	7
v0_00	%	0	0	0	1.097	2.262	14.925	21.304	32.937	26.476
v0_15	%	0	0	0	7.6754	23.756	24.016	33.227	54.365	43.619
v15_30	%	0	0	0	16.009	30.317	12.619	13.514	15.873	26.095
v30_50	%	0	0	3.695	31.14	31.448	23.202	25.755	21.032	23.238
v50_70	%	0	0	16.01	23.246	11.991	28.223	24.006	8.7302	7.0476
v70_90	%	3.771	27.713	39.655	13.816	2.489	9.091	3.498	0	0
v90_110	%	82.623	65.698	38.424	8.114	0	2.8494	0	0	0
v110_200	%	13.607	6.5891	2.2167	0	0	0	0	0	0
r100_25	%	0	0	0	0.879	0.227	0.544	0.478	0.398	0.191
r25_15	%	0	0	0.988	2.857	3.401	3.669	4.459	2.982	3.244
r15_10	%	0.493	0.388	0.988	4.396	3.175	6.386	5.414	3.977	5.534
r10_05	%	4.434	2.718	6.667	6.593	10.204	5.299	8.280	9.344	7.061
r05_0	%	35.304	38.447	32.593	27.033	20.862	19.565	18.312	11.928	13.931
a0_05	%	56.814	54.369	53.58	42.857	41.95	48.098	44.586	51.491	50.573
a05_10	%	2.627	3.301	4.691	11.868	13.832	8.696	10.987	11.133	10.878
a10_15	%	0.328	0.583	0.494	2.418	4.989	5.027	4.618	6.163	7.634
a15_25	%	0	0.194	0	1.099	0.907	2.717	2.707	2.386	0.954
a25_100	%	0	0	0	0	0.454	0	0.159	0.199	0
PKE	m/s ²	0.219	0.235	0.280	0.359	0.535	0.415	0.504	0.653	0.534
va_0	m ² /s ³	40.230	41.553	41.235	41.758	37.868	35.462	36.943	28.628	29.962
va0_3	m ² /s ³	23.974	19.029	15.309	25.934	38.776	36.277	38.376	52.883	51.718
va3_6	m ² /s ³	17.570	19.417	19.753	15.385	12.018	14.538	9.395	8.748	11.832
va6_10	m ² /s ³	8.210	12.039	16.296	13.187	5.669	9.239	9.713	6.163	4.962
va10_15	m ² /s ³	8.210	6.019	4.938	3.297	5.215	3.125	4.618	3.181	1.527
va15_99	m ² /s ³	1.806	1.942	2.469	0.440	0.454	1.359	0.955	0.398	0
va_avg	m ² /s ³	-0.129	0.221	-0.199	-0.478	0.248	-0.308	-0.478	-0.039	-0.089

Note: RT1, High-speed freeway; RT2, Freeway under LOS A-C; RT3, Freeway under LOS D; RT4, Freeway under LOS E; RT5, Freeway under LOS F; RT6, Arterial/Collector under LOS A-B; RT7, Arterial/Collector under C-D; RT8, Arterial/Collector under E-F; RT9, Local roadway.

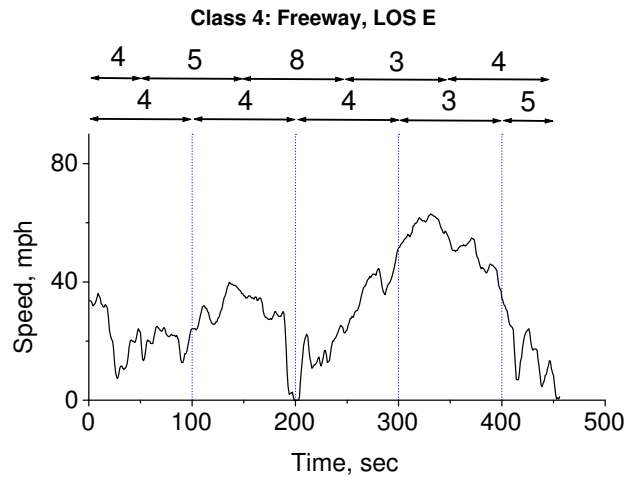


Figure 3.4 Validation of trained LVQ network on the freeway, LOS E drive cycle (Class 4)

order to remedy this situation each drive cycle was divided into an appropriate number of 150 second overlapping segments that constitute *subclasses* of the whole drive cycle (a *class*.) The rationale here is that the typical (stop-go-stop) cycle in urban traffic situations is approximately 3 minutes [38]. Thus the value of 150 sec, which is slightly less than 3 minutes, is used in this study.

With this in mind, overlapping drive cycle segments of 150 seconds each were used to form a training data matrix of $[141 \times 55]$ (See Fig. 3.5.) Note that $47 \times 3 = 141$ is the number of (transformed) parameters characterizing each driving pattern while 55 is the number of subclasses making up totally 9 classes; each class is made up of approximately 6 subclasses although the exact number of subclasses in each class varies, depending on the length of the drive cycle considered (See Table 3.5.)

Before proceeding, it is important to notice that the performance (the behavior of a network, commonly *mean squared error* of the network output) of the LVQ network can be affected by the number of neurons in the competitive layer (S^1). Likewise the value of α , used in the generation of the training data matrix, plays a role in the training performance of the network. In the case at hand, $\alpha = 0.55$ and $S^1 = 110$ or

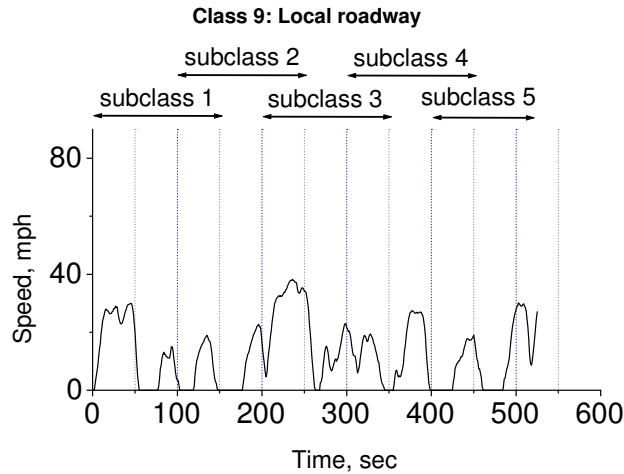


Figure 3.5 Training data generation: subclass and its class

twice the number of subclasses (drive cycle segments.)

The performance of the revised LVQ network is shown in Table 3.5. The table shows that the majority of the drive cycle segments were correctly classified, while a handful were not. The circled-numbers in the table indicate a mismatch in the classification compared with the target class. However, it should be noted that these mis-matched segments are likely the result of the similarity of the neighboring classes. For instance, statistics of the [200 ~ 350] segment in the arterial/collector LOS C-D cycle may not be distinguished from those of arterial/collector LOS E-F cycle. Thus the given segment is classified under Class 8. Similar mis-classifications are evident other cases such as the [0 ~ 150] segment of freeway LOS D drive cycle as well as the [300 ~ 450] segment of freeway LOS A-C drive cycle. The total number of mis-classifications, however, is rather small in comparison to the number of those properly classified.

It should further be noted that the RTI LVQ network exhibits a certain level of sensitivity to the length of the segment being identified. In particular, a network trained with 150 second segments will likely have a higher mis-classification rate on segments that are shorter than 150 second although it generally performs well on

Table 3.5 LVQ network result: MSE of the network, 0.0162; Size of S^1 , 110 ($= 2 \times 55$)

Class		Subclass							
		Full Data	0 – 150	100 – 250	200 – 350	300 – 450	400 – 550	500 – 650	600 end
1. Freeway, High-speed	Target class	1	1	1	1	1	1	1	N/A
	Network output	1	1	1	1	1	1	1	N/A
2. Freeway, LOS A-C	Target class	2	2	2	2	2	2	N/A	N/A
	Network output	2	2	2	2	①	2	N/A	N/A
3. Freeway, LOS D	Target class	3	3	3	3	3	N/A	N/A	N/A
	Network output	3	②	3	3	3	N/A	N/A	N/A
4. Freeway, LOS E	Target class	4	4	4	4	4	N/A	N/A	N/A
	Network output	4	4	4	4	4	N/A	N/A	N/A
5. Freeway, LOS F	Target class	5	5	5	5	5	N/A	N/A	N/A
	Network output	5	5	5	5	5	N/A	N/A	N/A
6. Arterial/Collector, LOS A-B	Target class	6	6	6	6	6	6	6	6
	Network output	6	6	6	6	6	6	6	6
7. Arterial/Collector, LOS C-D	Target class	7	7	7	7	7	7	7	N/A
	Network output	7	7	7	③	7	7	④	N/A
8. Arterial/Collector, LOS E-F	Target class	8	8	8	8	8	8	N/A	N/A
	Network output	8	8	8	8	8	8	N/A	N/A
9. Local Roadway	Target class	9	9	9	9	9	9	N/A	N/A
	Network output	9	9	9	9	9	9	N/A	N/A

Table 3.6 Description of driving trend

v_{avg}	a_{avg}	Description
L	Z	Low speed cruise
H	Z	High speed cruise
-	N or P	Acceleration/deceleration

Notes: L, Low; H, High; Z, Zero; N, Negative; P, Positive.

segments that are longer than this period.

3.3.2.2 Driving Trend Identifier (DTI)

While RTI is used to characterize the driving situation over a 100 to 150 second range, the purpose of Driving Trend Identifier (DTI) is to assess the *short term* or *transient features* of the drive cycle, such as low speed cruise, high speed cruise, acceleration/deceleration, and so on. These transient effects on driving *trends* can be described by the magnitudes of the average speed (v_{avg}) and acceleration (a_{avg}) values [39]. In this dissertation the following ranges of values for average speed and acceleration defining the trend of vehicle operation are defined as follows:

- Low speed cruise, $0 < v_{avg} \leq 36.66$ ft/s (25 mph), $-.5 \leq a_{avg} \leq .5$ ft/s²;
- High speed cruise, $v_{avg} > 58.65$ ft/s (40 mph), $-.5 \leq a_{avg} \leq .5$ ft/s²;
- Acceleration / Deceleration, $a_{avg} > .5$ / $a_{avg} < -.5$ ft/s².

As we shall see shortly, the assessment of DTI is used in the fuzzy torque distributor (as shown in Table 3.6.)

Its membership functions for average speed (v_{avg}) and acceleration (a_{avg}) are shown in Fig. 3.6.

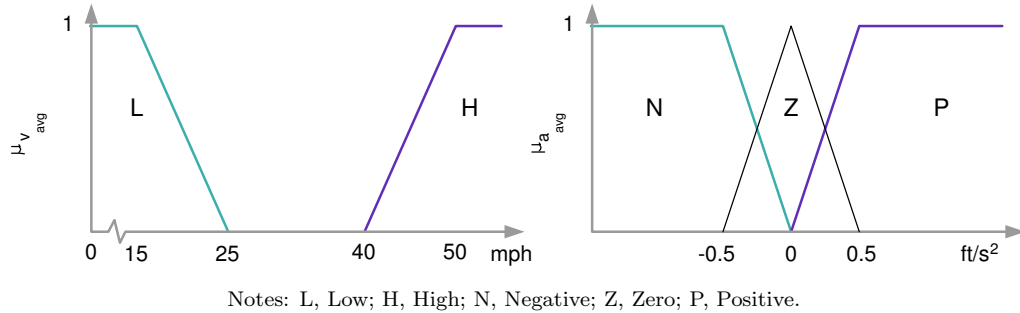


Figure 3.6 Membership functions in DTI

3.3.2.3 Driving Mode Identifier (DMI)

The *instantaneous* operating mode of the vehicle every second is the representation of the driver's intention (desire) for the operation of the vehicle, such as start-up, acceleration, cruise, deceleration (braking), and stationary. From the viewpoint of energy management for parallel hybrid vehicles, for each mode different energy management strategies are required to control the flow of energy in the drivetrain and maintain adequate reserves of energy in the electric energy storage device [14], consequently expecting improved performance. In this study, this idea is incorporated into IEMA through a driving mode identifier (DMI) with control strategies developed in the fuzzy torque distributor. Since the control of energy flow in the hybrid drivetrain directly affects vehicle mileage and emissions, its implementation into IEMA is requisite for enhancing the performance of the vehicle.

DMI determines what the current vehicle's operating mode is - *start-up, acceleration, cruise, deceleration, and/or stationary (stop or idle.)* The recognition of driving modes of the vehicle (in the fuzzy torque distributor) is made by examining the following torque relations on the drive shaft:

- Start-up: $|T_l| = 0, T_{dc} > 0$
- Acceleration: $|T_l| > 0, T_{dc} > 0$
- Cruise: $|T_l| > 0, T_{dc} = 0$
- Deceleration: $|T_l| > 0, T_{dc} < 0$
- Stationary: $|T_l| = 0, T_{dc} = 0$

Table 3.7 Description of driving mode

T_{dc}	N_E	Description
PB	Z	Start-up
PS/PB	L/H	Acceleration
Z	L/H	Cruise
N	-	Deceleration

Notes: L, Low; H, High; Z, Zero; N, Negative; PS, Positive Small; PB, Positive Big.

where $|T_l|$ is the torque required for maintaining the vehicle speed constant while overcoming the road load (rolling resistance, wind drag, and road grade.) T_{dc} is the torque required for acceleration or deceleration of the vehicle (driver's intention.) As we shall see later, the assessment of DMI is used in the fuzzy torque distributor (as shown in Table 3.7.)

Specifically, the engine speed (N_E) is used to infer the road load (T_l). The road load is a function of the road grade and the speed of the vehicle. Under the assumption that mechanical connection between the engine and the wheels through transmission converts the input argument for the speed of the vehicle to the engine speed, and driving occurs on a level road, the road load can be represented by the engine speed. Its membership functions for the driver's intention (T_{dc}) and the engine speed (N_E) are shown in Fig. 3.7.

3.3.2.4 Driver Style Identifier (DSI)

Driver style or behavior has a strong influence on emissions and fuel consumption [39]-[45]. In particular, [41] has identified three types of driving styles as follows:

- *Calm driving* implies anticipating other road user's movement, traffic lights, speed limits, and avoiding hard acceleration;
- *Normal driving* implies moderate acceleration and braking;

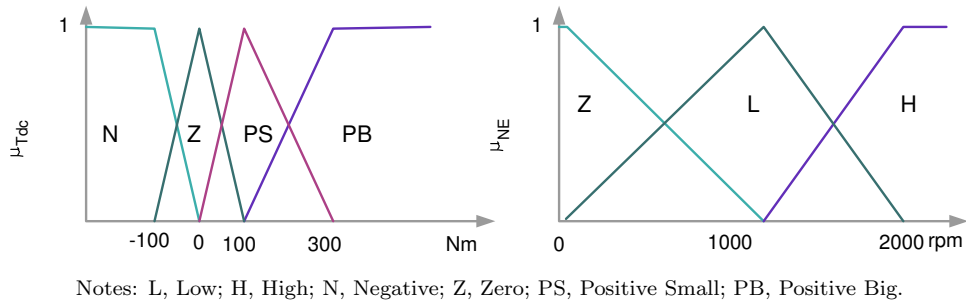


Figure 3.7 Membership functions in DMI

- *Aggressive driving* implies sudden acceleration and heavy braking.

Moreover, De. Vlieger et al., [41] notes that emissions obtained from aggressive driving in urban and rural traffic are much higher than those obtained from normal driving. A similar trend is observed in relation to fuel consumption. It is implied that the driving style affects the emissions rates and the fuel consumption rate, as does roadway type.

Fuzzy driving style identifier. In this study, average acceleration and standard deviation (SD) of acceleration over a specific driving range are used together to identify the driving style. (Most previous research uses only acceleration rate.) Acceleration criteria for the classification of the driver's style are based on the acceleration ranges proposed by De Vlieger et al. [41]. De Vlieger et al., defined the typical ranges of average accelerations² on a city journey for different driving styles: *Calm driving*, 1.48 ~ 2.13 ft/s²; *Normal driving*, 2.13 ~ 2.62 ft/s²; *Aggressive driving*, 2.79 ~ 3.61 ft/s². Again, for highway traffic average accelerations only ranged from 0.26 ~ 0.66 ft/s².

Standard deviation (SD) is one of indices of variability that can be used to characterize the dispersion among the measures in a given group of samples. In

²The values above were acquired from the experiments in Belgium involving different types of drivers and thus, it needs to be reconsidered for applicability in any other driving situation in different countries.

Table 3.8 Representation of driving style with acceleration and standard deviation

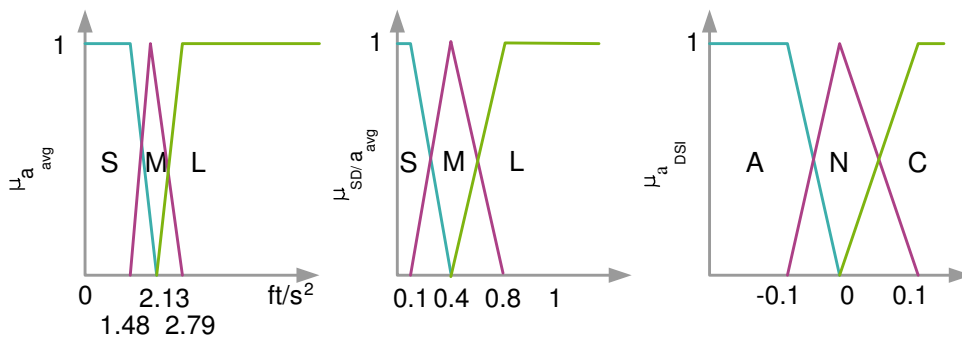
Driving Pattern	1	2	3
Accel. sample (ft/s ²)	{0.98 1.64 2.30}	{0.33 1.64 2.95}	{0.03 0.33 4.56}
\bar{a} (ft/s ²)	1.64	1.64	1.64
SD (ft/s ²)	0.66	1.31	2.53
$\frac{SD}{\bar{a}}$ (%)	40	80	154.3
Driving style	C	C/N	C/N/A

Notes: \bar{a} , average acceleration; SD, standard deviation of acceleration; C, Calm; N, Normal; A, Aggressive.

addition, it is conceptualized as an average distance among the measures with respect to the average value of the measures [46]. Since the value of SD of acceleration gives information on how far the samples of acceleration are dispersed with respect to the average acceleration, this is a valuable factor indicating the confidence level of acceleration occurrence around the average value of acceleration. In this study, the ratio of standard deviation to average acceleration, $\frac{SD}{\bar{a}}$ is used as a confidence measure of being the driving style that is classified by average acceleration.

As an example, let us say we have a driver with a value of average acceleration of 1.64 ft/s² (0.5 m/s²). It is not easy to say from this value that the driver's style is *calm*, when we refer to the ranges of acceleration values described above. For different values of SD with the same value of (average) acceleration, different styles of driver behavior may be inferred (See Table 3.8.)

With this in mind, a fuzzy DSI is designed with the membership functions defined in Fig. 3.8. The inputs to DSI are the value of average acceleration (\bar{a}) and the ratio of SD to average acceleration ($\frac{SD}{\bar{a}}$). The output of DSI, α_{DSI} , is a factor (weight) that compensates for the effect of a driving style on fuel consumption and emissions. Fuzzy rule set for the operation of DSI is shown in Table 3.9.



Notes: S, Small; M, Medium; L, Large; C, Calm; N, Normal; A, Aggressive.

Figure 3.8 Membership functions in DSI

Table 3.9 Rule set for fuzzy DSI

	$\frac{SD}{\bar{a}}$		
	S	M	L
\bar{a}	S C C N	M N N A	L A A A

Notes: S, Small; M, Medium; L, Large; C, Calm; N, Normal; A, aggressive.

3.4 Intelligent Energy Management Strategies

Energy management in HEVs aims at minimizing fuel consumption and pollutant emissions. To achieve this goal, an energy management system should address two issues: when and how much propulsive power should be generated (torque distribution operation); when and how the charge sustenance operation should be carried out.

The following torque balance equation illustrates the energy management concept adopted in this study.

$$\underbrace{T_e + \overbrace{T_{ec,FTD}}^{\text{propulsion}} + \overbrace{T_{ec,SOC}}^{\text{charging}}}_{\text{Engine}} + \underbrace{T_{mc}}_{\text{Motor}} = T_c \quad (\text{Revisited})$$

A fuzzy torque distributor proposed in this study is called upon for torque (power) distribution operation, and again, a vehicle-mode-based state-of-charge(SOC) compensator is designed for the charge sustenance operation. Details on the fuzzy torque distributor and SOC compensator are given in subsequent sections.

3.4.1 Fuzzy Torque Distributor (FTD)

3.4.1.1 Overview

Development of FTD is aimed for generating proper engine torque ($T_{ec,FTD}$) for propulsion in a way that promotes energy saving, resulting in *eco-driving* while satisfying the driver's demand.

In this study, achievement of this goal is made by proposing a concept of “driving situation awareness”-based torque distributor and by incorporating this into IEMA. This concept is based on the idea that the driving environment can affect fuel consumption and pollutant emissions as well as the modes (and trends - modal transitions) of operation of the vehicle. The driving environment mentioned here can be understood as a situation that demands a specific operating mode of the vehicle or makes the vehicle to perform a specific driving trend.

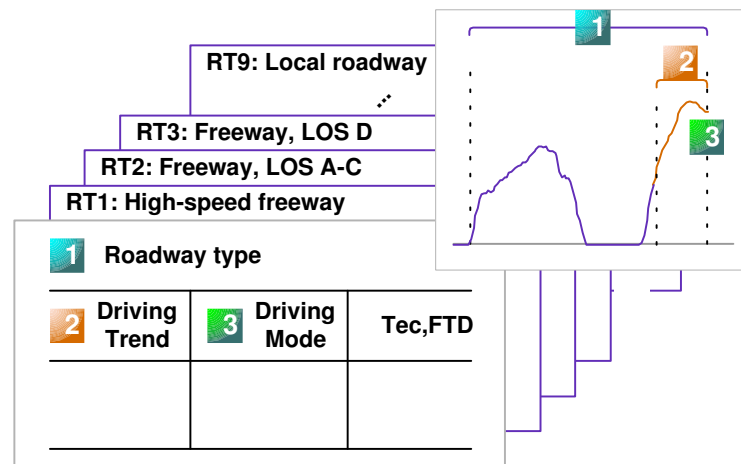


Figure 3.9 Structure of FTD rule base

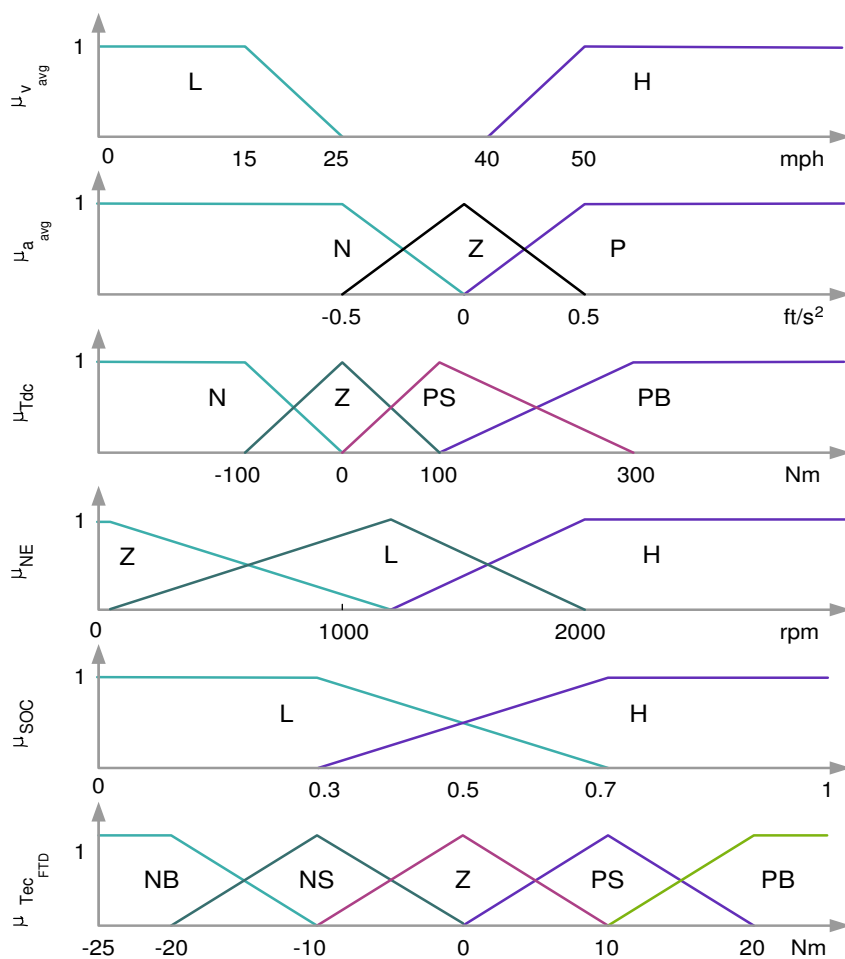
In order to implement this idea, the structure of FTD was determined as shown in Fig. 3.9. Rule base within FTD is the representation of the expert knowledge (of skilled drivers) that characterizes the relationship between the driving situation and energy flow in the hybrid drivetrain.

Rule firing process inside FTD is as follows: According to the facility type identified from RTI, one of nine facility-based rule bases indexed by RT1 through RT9, as shown in Fig. 3.9, which forms a counterpart with the facility type, is selected and fired based on the information about the operating modes and trends of the vehicle. Membership functions for FTD are shown in Fig. 3.10.

3.4.1.2 Preliminary Concepts for Rule Base Design

Fuzzy rule base development starts with the postulate that fuel economy in HEVs operation can be achieved by operating the ICE at the efficient region of the engine and by avoiding transient operations that would occur in a driving situation such as abrupt acceleration and/or deceleration, frequent stop-and-go event, and so on.

Through the literature survey [31], [32], [39]-[42], and [47], I investigated the



Note: P, Positive; N, Negative; PS, Positive Small; PB, Positive Big; Z, Zero; NS, Negative Small; NB, Negative Big; L, Low; H, High.

Figure 3.10 Membership functions in FTD

driving pattern factors that affect fuel consumption and emissions and that would be used in the development of the fuzzy rule base. Fig. 3.11, in particular, describes fuel consumption rate of the passenger car as function of average speed of the vehicle [47]. The vertical lines on the plots indicate the vehicle speed operating range on the facility-specific drive cycles in terms of $[v_{avg} - v_{std}, v_{avg}, v_{avg} + v_{std}]$. Again, Fig. 3.12 gives a graphic view of factors affecting emissions and fuel consumption addressed in [31] for each of 9 facility-specific drive cycles, which together with Fig. 3.11 are used in the fuzzy rule base development in FTD.

As shown in Fig. 3.9, the rule base consists of facility-specific rule sets devised for optimal energy management for a given facility type. The rationale underlying each rule set is given below.

3.4.1.3 Low Speed Cruise Trend

The speed range of the low-speed-cruise regime defined in this study is below 36.66 ft/s (25 mph) with small acceleration/deceleration rates (within ± 0.5 ft/s²). In order to maximize fuel economy in this regime, the following strategy is adopted here: When the level of the SOC is high, the electric motor (EM) is used to provide the propulsive power to the vehicle to meet the driver's intention (T_{dc}). On the other hand, when the SOC is low, the ICE is used to generate propulsive power even if it means high fuel consumption; priority is given to maintaining the SOC. For low speed region of the ICE under low SOC, no additional engine operation for propulsion is made to avoid the ICE operation at inefficient regions of the engine. For high engine speed under low SOC, the ICE, together with the EM, are used to generate propulsive power. This strategy is applied to all facility-specific drive cycles whenever this driving trend is present. Fuzzy rule base for this trend is in Table 3.10.

3.4.1.4 High Speed Cruise Trend

Vehicle speed range defined for "high speed cruise" in this study covers speeds of over 58.65 ft/s (40 mph) with a small acceleration/ deceleration rates (within ± 0.5 ft/s²).

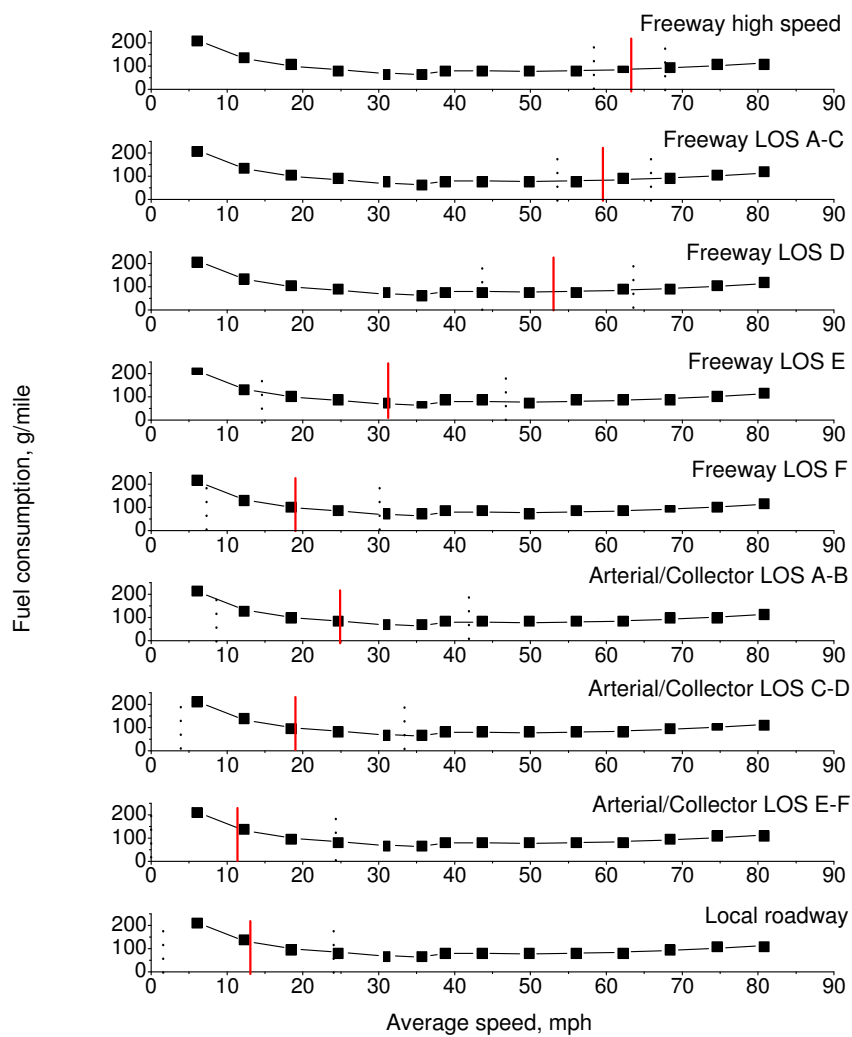
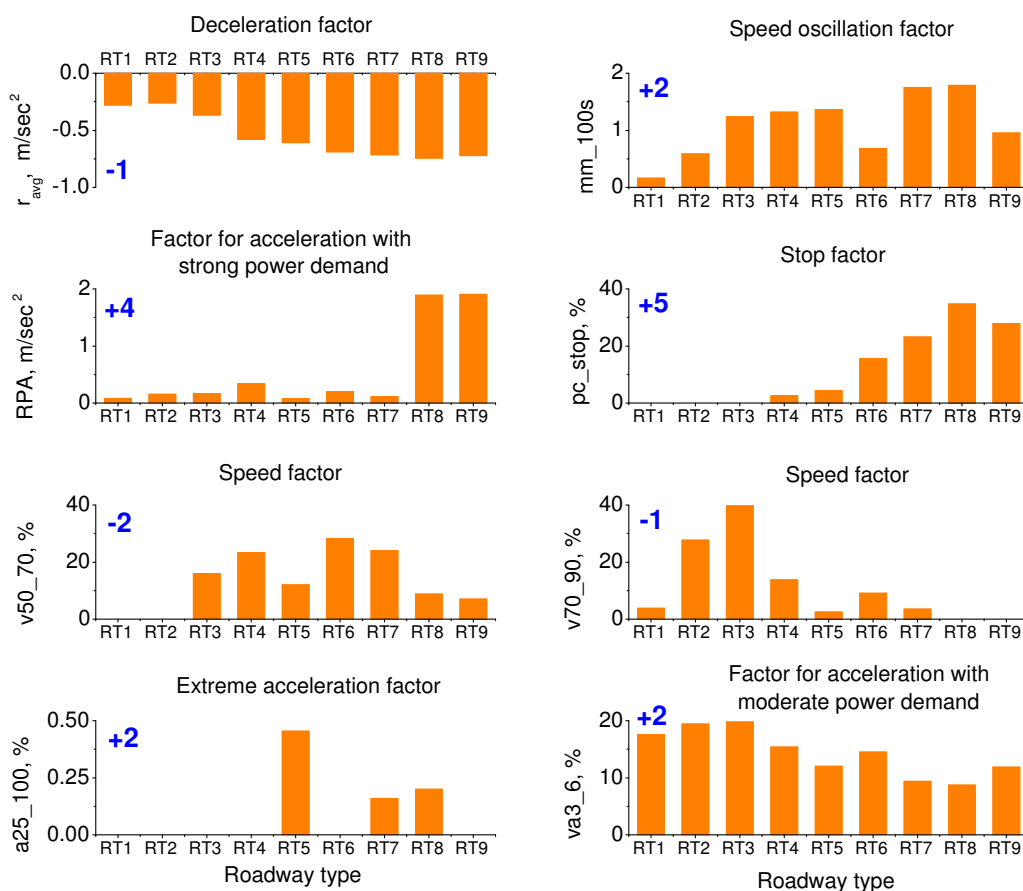


Figure 3.11 Fuel consumption rate as function of average speed for passenger car (Vehicle operating speed range $[v_{avg} - v_{std}, v_{avg}, v_{avg} + v_{std}]$ for facility-specific drive cycles)



Note: RT1, High-speed freeway; RT2, Freeway under LOS A-C; RT3, Freeway under LOS D; RT4, Freeway under LOS E; RT5, Freeway under LOS F; RT6, Arterial/Collector under LOS A-B; RT7, Arterial/Collector under C-D; RT8, Arterial/Collector under E-F; RT9, Local roadway.
 '+' sign with number (intensity) indicates how factors affect fuel economy adversely.

Figure 3.12 Representative factors affecting emissions and fuel consumption in each facility-specific drive cycle

Table 3.10 Rule base of the FTD: low-speed cruise trend

	DMI			FTD
	T_{dc}	N_E	SOC	$T_{ec,FTD}$
Start-up	N/A			
Acceleration	PS	L	H	NS
	PB	L	H	NB
	PS	H	H	NS
	PB	H	H	NB
	PS	L	L	Z
	PB	L	L	Z
	PS	H	L	PS
	PB	H	L	PB
Cruise	Z	L	H	Z
	Z	H	H	NS
	Z	L	L	Z
	Z	H	L	PS
Deceleration	N			NB
Stationary	N/A			

Notes: PS, Positive Small; PB, Positive Big; Z, Zero; NS, Negative Small; NB, Negative Big; L, Low; H, High.

Since this trend is characterized as a high and broad speed range with small acceleration rate, the ICE is used to provide propulsive power in speed range consistent with efficient engine operation. For speeds over 55 mph, the fuel consumption rate again increases with the increase of vehicle speed (as shown in Fig. 3.11.) In this region, the EM is used to lessen the overall fuel usage. Continued use of the EM, however, results in the SOC compensator acting to recover the SOC of the battery. Another reason for the EM operation is to provide power to cope with high power demand due to the wind drag that would be beyond the capability of the ICE in a high-speed region. Again, this strategy is applied to all facility-specific drive cycles whenever this driving trend is present.

Depending on the gear ratio during driving, the engine speed is determined according to the speed of the vehicle. Given the speed of the vehicle, the engine speed will be high or low depending on the gear ratio. For high speed region of the engine, the ICE is allowed to generate power according to the level of SOC. The EM usage is again allowed for low speed region of the engine (See Table 3.11 for fuzzy rule base for high-speed cruise trend.)

3.4.1.5 Acceleration/deceleration Trend

In the acceleration/deceleration regime, fuzzy rule base is devised based on the characteristic features of each drive cycle (i.e., each of 9 facility-specific drive cycles,) and is derived by comparing with the characteristics of neighboring drive cycles. Rule base development in acceleration/deceleration regime follows the same notion in low/high-speed cruise regime with a trade-off between the ICE and the EM usage associated with factors affecting emissions and fuel consumption for each drive cycle considered in this study (See Table 3.12 for fuzzy rule bases for acceleration/deceleration trend.)

Freeway, high-speed cycle (RT1). Under a driving environment allowing the vehicle to be accelerated in high-speed driving, such as highway driving, the magnitude of acceleration (/deceleration) rate would be relatively small when the driver presents his/her intention to accelerate more. This implies no hard acceleration or deceleration

Table 3.11 Rule base of the FTD: high-speed cruise trend

		DMI			FTD
		T_{dc}	N_E	SOC	$T_{ec,FTD}$
Start-up		N/A			
Acceleration	PS	L	H	NB	
	PB	L	H	NB	
	PS	H	H	PS	
	PB	H	H	PS	
	PS	L	L	NS	
	PB	L	L	NS	
	PS	H	L	PB	
	PB	H	L	PB	
Cruise	Z	L	H	NB	
	Z	H	H	PS	
	Z	L	L	NS	
	Z	H	L	PB	
Deceleration	N			NB	
Stationary		N/A			

Notes: PS, Positive Small; PB, Positive Big; Z, Zero; NS, Negative Small; NB, Negative Big; L, Low; H, High.

will be present in high-speed driving. From the observation on statistics shown in Table 3.4, it can be seen that the characteristics of high-speed driving, such as the high-speed freeway cycle, is similar to those of driving under high-speed cruise regime, except for the difference in the speed range of the vehicle operation: The speed region of the vehicle operation in high-speed freeway cycle is very narrow compared with those of driving under high-speed cruise regime, but with highest speed on the average (See also Fig. 3.11.)

In light of this observation, the rule base for this cycle can be derived from the rule base for driving on high-speed cruise regime (in Table 3.11) by considering the difference in the driving characteristics of these regimes: Except that the usage of the ICE is restricted to some extent due to the high speed characteristics giving high fuel consumption rate on the high speed region of the engine ($N_E = \text{“H,”}$) the same strategy as for high-speed cruise regime is applied for this cycle.

Freeway, LOS A-C cycle (RT2). The fuzzy rule base for the freeway, LOS A-C cycle has the same format as those for the high-speed freeway cycle, since the statistics of both drive cycles are close to each other and there is no significant difference between them from the viewpoint of engine operation.

Freeway, LOS D cycle (RT3). In the freeway, LOS D cycle, the speed band of the vehicle operation is shifted down to some extent (compared with the freeway, LOS A-C cycle,) while overlapping the efficient region of the vehicle speed in terms of fuel consumption rate (See Fig. 3.11.) In addition, the operating range of the ICE may be in the range that the ICE can cover the road load demand depending on the gear ratio.

The main difference in this cycle compared with the freeway, LOS A-C cycle (RT2) is the increase in the value of the *speed oscillation factor* in terms of the parameters [31]: mm_{100s} ; lmm_{100s} ; lmm_{100m} ; PKE; mm_{100m} (See Appendix A for their meanings.)

The vehicle being driven on this cycle characterized by the *speed oscillation factor* may experience frequent speed changes represented by the frequent application of

acceleration and/or brake pedal. Thus, this factor would affect fuel consumption when the ICE is used on this cycle by causing transient behavior of the engine. With this in mind, our strategy for driving on this drive cycle is as follows. The usage of the ICE is restricted to some extent compared with RT2 when the driver's intention (T_{dc}) and the speed of the engine are high. When T_{dc} is zero ($T_{dc} = \text{"Z,"}$) the same fuzzy rules for RT2 are adopted, since the driver's intention for acceleration or deceleration is zero or small as shown in RT2 cycle.

Freeway, LOS E cycle (RT4). The speed variability of the vehicle operation in the freeway, LOS E cycle is broad from low speed to high speed region, while overlapping the efficient region of vehicle speed for the use of the ICE.

The adopted strategy for driving on this cycle is as follows. When the engine speed is high ($N_E = \text{"H,"}$) the ICE is used to provide propulsive power together with the EM (i.e., the increment of engine torque, $T_{ec,FTD}$ is set as "PS" or "PB" in proportion to the magnitude of the driver's intention, T_{dc}) to take full advantage of low fuel consumption in that region. When the engine speed is low ($N_E = \text{"L,"}$) it is expected that the EM is used. This strategy is adopted to avoid high fuel consumption at low speed region of the engine, and to generate high propulsive power from the EM at low speed region of the vehicle. Furthermore, the amount of the EM used is determined according to the level of the SOC.

Freeway, LOS F cycle (RT5). This cycle is characterized as the most congested traffic situation on the freeway. The speed band of the vehicle operation in the freeway, LOS F cycle is positioned at low speed region where the fuel consumption rate is very high (See Fig. 3.11.) Again, the *extreme acceleration factor* (represented by $a_{25,100}$; See Appendix A) is high compared with other cycles as shown in Fig. 3.12.

In light of this observation, the rule base of this cycle is developed as follows: When the engine speed is low ($N_E = \text{"L,"}$) the EM is used (for propulsion) to avoid excessive fuel usage that would occur when the ICE used, although this causes the battery's SOC to drop down (Note that the charge sustaining operation, however, is carried out simultaneously according to the current level of SOC.) The amount of

the EM usage in the high speed region of the engine is determined by considering the effect of the *extreme acceleration factor* of this cycle. For example, the use of the EM is enforced when the driver's demand for acceleration is high ($T_{dc} = \text{"PB"}$) under high engine speed (NE = "H") and high SOC (SOC = "H.")

Arterial/collector, LOS A-B cycle (RT6). The speed characteristics in the arterial/collector, LOS A-B cycle is similar to those of the freeway, LOS E cycle (RT4), with the speed band shifted down to some extent.

The basic strategy for driving on this cycle is to follow the strategy for the freeway, LOS E cycle, while considering the differences in terms of transient behavior of the ICE. The main differences between the two drive cycles are the decrease of the *speed oscillation factor* and the increase of the *stop factor* (Note that these factors are defined in Appendix A.) Both factors would adversely affect fuel consumption when the ICE is used (as indicated by the number at each plot in Fig. 3.12.) With this in mind, the usage of the ICE is replaced with those of the EM in the high speed region of the engine.

Arterial/collector, LOS E-F cycle (RT8). As shown in Fig. 3.12, this cycle presents the low speed characteristics, most frequently stop and go, abrupt acceleration and deceleration rates, and high power demand as well as the lowest average speed among the 9 facility-specific drive cycles at hand.

The speed characteristics of driving on this drive cycle is similar to those of driving under low-speed-cruise regime. The main difference in this cycle compared with the low-speed- cruise regime is the magnitude of the acceleration rate: $[a_{avg}, a_{std}] \sim [0, 0]$ in driving under low-speed-cruise regime; $[a_{avg}, a_{std}] \gg [0, 0]$ in driving on the arterial/collector, LOS E-F cycle.

From the above observation, the strategy for driving on this cycle follows those of driving under low-speed-cruise regime (in Table 3.10,) with the suggestion that the EM be used to avoid transient behavior of the engine.

Arterial/collector, LOS C-D cycle (RT7). The rule base for the arterial/ collector, LOS C-D cycle is derived by revising the effect of *factor for acceleration with strong power demand* in the arterial/collector, LOS E-F cycle (RT8) (See Fig. 3.12.) This factor, as described in [31], measures the existence of high power demand and the magnitude of acceleration in the drive cycle at hand. Some parameters being comprised in this factor are: Relative Positive Acceleration ($RPA = \frac{1}{x} \int va^+ dt$, $a^+ = \frac{dv}{dt} > 0$, x = travel distance); % of time when $va > 10 \text{ m}^2/\text{s}^3$; % of time when a is $0.5 \sim 1.5 \text{ m/s}^2$; % of time when a is $1.5 \sim 2.5 \text{ m/s}^2$; and so on. One of the main parameters representing this factor is the RPA.

As shown in Fig. 3.12, the effect of *factor for acceleration with strong power demand* in this cycle on fuel consumption is *small* compared with RT8 cycle. The small value in the magnitude of RPA is understood as two cases: (1) the magnitude of the speed during acceleration (a^+) is small; and/or (2) the magnitude of acceleration (a^+) is small during driving through the total travel distance.

For this cycle, the magnitude of average acceleration of the cycle is relatively large compared to other cycles at hand and no significant difference is found compared to RT8 cycle (See Table 3.4.) In light of this observation, it is implied that the small RPA of this cycle may be due to the first case mentioned above; consequently, the vehicle is intended to be accelerated (probably with high rate) in the low speed region of the vehicle only.

It is conceived from the observation that the magnitude of acceleration in the high speed region of the vehicle is relatively small and the speed band of this cycle is overlapping with the efficient region of the operation of the vehicle in high speed region. With this in mind, the ICE can be used in the high-speed region of the engine for propulsive power together with the EM, compared with the rule sets for RT8.

Local roadway cycle (RT9). The speed characteristics of local roadway drive cycle is similar to those of arterial/collector, LOS E-F cycle (RT8) from the viewpoint of the engine operation. While the *speed oscillation factor*, the *stop factor*, and the *extreme acceleration factor* are reduced, the *factor for acceleration with moderate power demand* increases to some extent in this cycle. The representative value of the

Table 3.12 Rule base of the FTD: acceleration/deceleration trend

DMI				RT1	RT2	RT3	RT4	RT5	RT6	RT7	RT8	RT9
T_{dc} N_E SOC				$T_{ec,FTD}$								
Start-up	PB	Z		Z	Z	Z	Z	Z	Z	Z	Z	Z
Acceleration	PS	L	H	NB	NB	NB	NS	NB	NS	NS	NS	NS
	PB	L	H	NB	NB	NB	NB	NB	NB	NB	NB	NB
	PS	H	H	Z	Z	Z	PS	Z	Z	Z	NS	NS
	PB	H	H	Z	Z	NS	PB	NS	Z	NS	NB	NS
	PS	L	L	NS	NS	NS	Z	NB	Z	NS	NS	NS
	PB	L	L	NS	NS	NS	NS	NB	NS	NS	NS	NS
	PS	H	L	PS	PS	PS	PS	PS	Z	PS	Z	Z
	PB	H	L	PS	PS	Z	PB	PS	Z	PB	PS	PB
Cruise	Z	L	H	NB	NB	NB	NS	NB	NS	Z	Z	Z
	Z	H	H	Z	Z	Z	PS	Z	Z	Z	NS	NS
	Z	L	L	NS	NS	NS	Z	NB	Z	Z	Z	Z
	Z	H	L	PS	PS	PS	PS	PS	Z	PB	PS	PS
Deceleration	N			NB	NB	NB	NB	NB	NB	NB	NB	
Stationary	Z	Z		Z	Z	Z	Z	Z	Z	Z	Z	

Notes: P, Positive; N, Negative; PS, Positive Small; PB, Positive Big; Z, Zero; NS, Negative Small; NB, Negative Big; L, Low; H, High; RT1, Freeway High-speed; RT2, Freeway, LOS A-C; RT3, Freeway, LOS D; RT4, Freeway, LOS E; RT5, Freeway, LOS F; RT6, Arterial/Collector, LOS A-B; RT7, Arterial/Collector, LOS C-D; RT8, Arterial/Collector, LOS E-F; RT9, Local Roadway.

extreme acceleration factor, a_{25-100} (percent of time in acceleration interval $2.5 \sim 10$ m/s²) is zero. This implies that the effect of high acceleration on fuel consumption is very small even when the ICE is used. Since the overall speed band of this drive cycle is positioned at the low-speed region of the vehicle operation, it is best not to use the ICE to avoid excessive fuel consumption. With this in mind, when the engine speed is high ($N_E = \text{“H”}$) and the driver’s intention is high ($T_{dc} = \text{“H”}$) it can be intended for the ICE to be used, compared with the arterial/collector, LOS E-F cycle (but not mandatory.)

3.4.2 Drive Style Compensation

As stated in Section 3.3.2.4, the Driver Style Identifier (DSI) identifies the driver's style of driving by utilizing the information about the driving situation from DIE. The output of DSI is a driving style factor, α_{DSI} , which characterizes the driving style of the driver.

In this study, the design of DSI is proposed so that the effect of the driving style is compensated in the output of the fuzzy torque distributor (FTD). The compensation is carried out by multiplying by a factor (weight) which would characterize the driving style of a driver; i.e., the increment of the engine torque from FTD is adjusted in the following manner:

$$T_{ec,TD} = T_{ec,FTD} \times (1 + \text{sgn}(T_{ec,FTD}) \cdot \alpha_{DSI}) \quad (3.2)$$

where $T_{ec,FTD}$ is determined at FTD and $T_{ec,TD}$ is the increment of the engine torque compensating for the effect of driver variability. α_{DSI} is a weight that indicates driving style and gives how much engine torque should be added to (or subtracted from) $T_{ec,FTD}$ to compensate for the effect of driver variability.

This compensation can be justified as follows: Under the assumption that the transient operation of the engine yields much fuel consumption than steady operation does, the effect of a driver's behavior on the engine operation is considered. For example, for the aggressive driver, less use of the ICE is allowed to avoid fuel consumption that would occur due to the transient operation of the engine by the driver.

In this study, maximum 10% of the increment of engine torque is considered for calm (+10%) through normal (0%) to aggressive (−10%) driving. Notice that typical value of 10% is used here, however, the effect of this value on the overall performance should be addressed.

From (3.2), torque balance equation in (3.1), is modified as follows:

$$\underbrace{T_e + \overbrace{T_{ec,FTD} \times (1 + \text{sgn}(T_{ec,FTD}) \cdot \alpha_{DSI})}^{\text{propulsion}}}_{\text{Engine}} + \overbrace{T_{ec,SOC}}^{\text{charging}} + \underbrace{T_{mc}}_{\text{Motor}} = T_c \quad (3.3)$$

3.4.3 SOC Compensator (SCC)

In principle, the commanded output for the HEV operation from the torque distribution operation cannot guarantee the sustenance of the charge of the battery over the unknown range of driving to which the vehicle may subject. To facilitate the extension of the driving range, the level of electric energy available through the electric energy storage must be maintained within a prescribed range throughout driving. In this study, a state-of-charge compensator (SCC) is proposed and incorporated in IEMA to achieve the goal of the charge sustenance task.

The State-of-Charge Compensator enables this task to be carried out by detecting the current SOC and comparing with the target SOC, and commanding additional engine torque command ($T_{ec,SOC}$). As shown in (3.3), the increment of the engine torque from SCC ($T_{ec,SOC}$) is added to (or subtracted from) the current engine torque for the charge (or discharge) operation together with the increment of the engine torque for propulsive operation from FTD and DSI ($T_{ec,TD}$) for HEV operation.

3.4.3.1 Battery Charge Operation

Battery discharge/charge operation in HEVs experiences its duty cycle depending on the vehicle's mode of operation. A generic understanding of battery operation in HEVs is as follows. Battery charge in deceleration mode is mainly due to the regenerative-braking process and follows the braking pattern of the driver. In the acceleration mode, as well as non-level road driving mode, such as up-hill climbing, power from the battery is used together with the engine power to cope with the high-power demand, consequently resulting in discharge operation. When the vehicle is driving at a constant speed, a small amount of torque is needed to maintain the vehicle speed and to overcome the road load. Both power sources can be utilized to provide the power required in the cruise mode. Under the charge sustenance concept, the function of the electric motor can be switched to that of a generator to charge the battery for the next use if surplus power from the engine is available. In the driving mode, including acceleration and cruise mode, additional battery charge by

operating the ICE is not suggested because it may cause the overall performance to deteriorate and/or the battery to be overcharged. Selective battery charge operation may be needed for the operation of HEVs in these modes. In the stop (idle) mode, charge sustaining operation can be accomplished in an efficient region of the engine while maximizing fuel efficiency if applicable or required. While not considered in this study, external charge operation can be accomplished in the stationary (parking) mode of the vehicle. Details of charge sustaining strategies in both hybrid mode (acceleration, cruise, and deceleration) and stop mode are described as follows:

3.4.3.2 Charge Sustaining Strategy in Hybrid Mode

In this study, charge sustaining strategy in both hybrid and stop modes is proposed. The basic idea to maintain the SOC within a predetermined range is to command the engine and the motor to produce (additionally) more or less torque according to the current SOC of the battery. This idea is explained on the engine-motor torque plane, where the torque balance equation ($T_{ec} + T_{mc} = T_c$) is represented with respect to the motor and engine torque *at a given speed of the vehicle*. The points on the line describing torque balance equation represents the solution set that meets the driver's torque demand (See Fig. 3.13:)

$$\underbrace{T_e + \overbrace{T_{ec,TD}}^{\text{propulsion}}}_{T_{ec,1}} + \underbrace{T_{mc}^*}_{T_{mc,1}} = T_c \Leftrightarrow \underbrace{T_e + \overbrace{T_{ec,TD}}^{\text{propulsion}} + \overbrace{T_{ec,SOC}}^{\text{charging}}}_{T_{ec,2}} + \underbrace{T_{mc}^* - \overbrace{T_{ec,SOC}}^{\text{charging}}}_{T_{mc,2}} = T_c \quad (3.4)$$

where $T_{ec,TD}$ is the increment of engine torque compensated for the driving style effect (α_{DSI}). T_{mc}^* is motor torque which together with engine torque ($T_e + T_{ec,TD}$) meets the driver's torque command. For instance, in case the current SOC is below the target SOC and the charge sustaining operation is requested, generation of additional engine torque beyond that requested from the torque distribution operation ($T_{ec,TD}$) is enforced. The portion of additional engine torque is utilized to charge the battery by lessening the load on the motor that would otherwise deplete the battery's electric energy to overcome the load. In case that the current SOC is above the upper bound

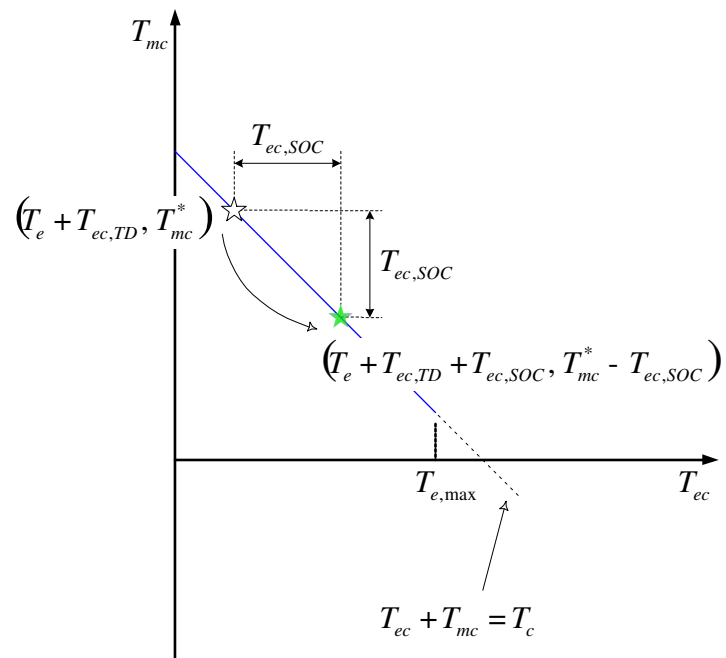


Figure 3.13 Illustration of charge sustaining operation

Table 3.13 Sectional division of the engine-motor torque plane

Section	Torque relation
1	$T_{m,max} < T_c \leq T_{e,max} + T_{m,max}$
2	$T_{e,max} < T_c \leq T_{m,max}$
3	$0 < T_c \leq T_{e,max}$
4	$T_{m,min} + T_{e,max} < T_c \leq 0$
5	$T_{m,min} \leq T_c \leq T_{m,min} + T_{e,max}$

Note: $T_{m,max}$, Maximum motor torque; $T_{e,max}$, Maximum engine torque; T_c , driver's torque command; $T_{m,min}$, Minimum motor torque.

of the SOC limit, the SOC level can be guided to the target SOC in a converse manner.

In order to accomplish the charge sustaining operation, one needs to control the amount of engine torque generation. The mission of the charge sustenance task is to calculate the increment of engine torque, $T_{ec,SOC}$, based on the deviation of the SOC from the target SOC (\overline{SOC}), ΔSOC , the increment of engine torque from FTD, $T_{ec,TD}$, as well as the current status of each component.

The SOC deviation (ΔSOC) is defined and normalized as follows:

$$\overline{SOC} = \frac{SOCH + SOCL}{2}, \Delta SOC = \overline{SOC} - SOC, N = -\frac{2 \cdot \Delta SOC}{SOCH - SOCL} \quad (3.5)$$

where “ $N = -1$ ” implies the current SOC hits the lower bound and “1” the upper bound. $SOCH$ and $SOCL$ represent high and low SOC limits, respectively.

According to the amount of the driver's torque demand, the engine-motor torque plane is divided into 5 sections, as shown in Table 3.13 (See also Fig. 3.14(a).)

At each section, the (engine) torque margin for the charge operation (TMC) and the discharge operation (TMD) are determined according to the mechanical and electrical limitations (to engine and motor torque) of the two powertrain components, and

the increment of engine torque from the torque distribution operation (See Fig.3.14 (b)-(d).) The torque margin defined here can be understood as the amount of change in engine torque allowed for the charge/discharge operations without violating the physical constraints governing primary power sources.

The increment of engine torque can be obtained by introducing an appropriate function that relates $T_{ec,SOC}$, the current SOC, TMC, and TMD:

$$T_{ec,SOC} = f(SOC, TMC, TMD)$$

For instance, the following logic may be used to define $f(\cdot)$ as a saturation function, which we believe is appropriate in the current context (See. Fig. 3.15.)

Case 1: Charge operation ($N < 0$)

$$T_{ec,SOC} = \begin{cases} TMC \cdot (-N) & \text{if } spc \leq N; \\ TMC & \text{if } N < spc; \end{cases}$$

Case 2: Discharge operation ($N > 0$)

$$T_{ec,SOC} = \begin{cases} -TMD \cdot (N) & \text{if } N \leq spd; \\ -TMD & \text{if } spd < N; \end{cases}$$

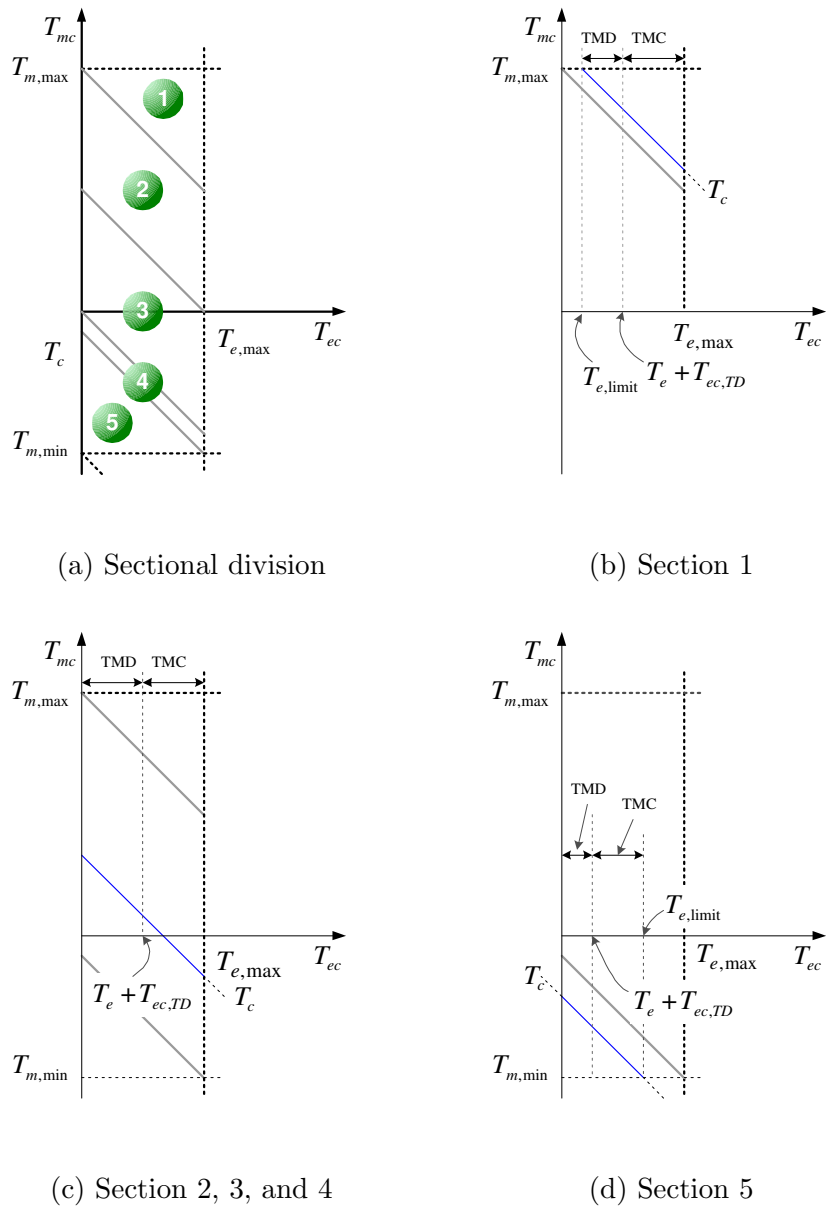
Case 3: ($N = 0$)

$$T_{ec,SOC} = 0$$

where spd and spc are user defined parameters. Typical values of these are 0.5, respectively.

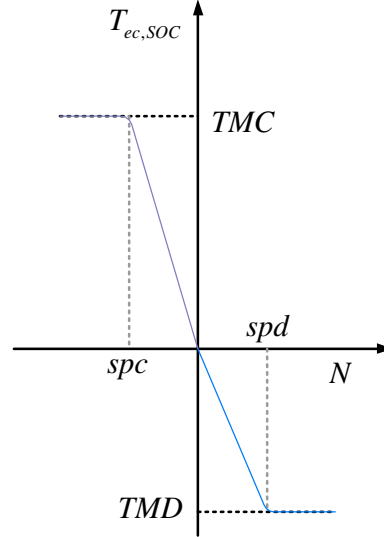
3.4.3.3 Charge Sustaining Strategy in Stop Mode

The charge sustaining operation in the stop mode is accomplished in a similar manner, as discussed above, except that the vehicle is at zero speed and no driver torque



Note: $T_{m,max}$, Maximum motor torque; $T_{e,max}$, Maximum engine torque; T_c , driver's torque command; $T_{m,min}$, Minimum motor torque; T_{mc} , Motor torque command; T_{ec} , Engine torque command; T_e , Current engine torque; $T_{ec,TD}$, Increment of engine torque for propulsion.

Figure 3.14 Definition of torque margins on the engine-motor torque plane



Note: $T_{ec,SOC}$, Increment of engine torque for charging; N , Normalized SOC index; TMC , Torque margin for charge; TMD , Torque margin for discharge; spc , spd , User defined parameters.

Figure 3.15 Saturation function for charge sustaining operation

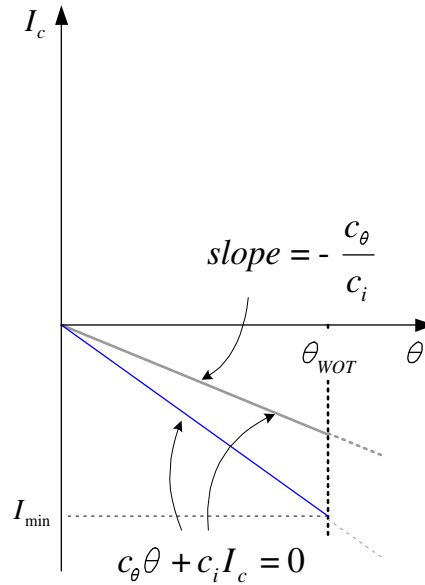
demand exists. In the stop mode, the charge sustaining operation is done in an *efficient* region of the engine while maximizing fuel economy. The main problem is to find the best point (or region) of operation of the engine and the continuously variable transmission (CVT) gear ratio so that engine efficiency is maximum.

To this end, as a preliminary step, the torque balance equation is approximated by the following form:

$$T_{ec} + T_{mc} = T_c \Leftrightarrow \underbrace{c_{\theta}(\omega, i_{CVT}) \times \theta}_{T_{ec}} + \underbrace{c_i(\omega) \times I_c}_{T_{mc}} = T_c \quad (3.6)$$

where $c_{\theta}(\omega, i_{CVT}) = \frac{T_{e,max}(\omega, i_{CVT})}{\theta_{WOT}}$; θ is the throttle setting of the engine and θ_{WOT} is the Wide-Open-Throttle; $T_{e,max}$ is the maximum engine torque; I_c is the electric current of the motor; ω is the drive shaft speed, and i_{CVT} is the gear ratio in the CVT. $c_i(\omega)$ is a vehicle speed dependent constant which makes electric machine torque by multiplying by the electric current.

This characteristics of the torque balance relation in (3.6) is well described on the



Note: I_c , Motor current; θ , Throttle setting; θ_{WOT} , Wide-Open-Throttle; c_θ , Engine torque constant; c_i , Motor torque constant.

Figure 3.16 Representation of torque balance constraint in the stop mode

throttle-current plane (θI_c -plane) shown in Fig. 3.16. The torque balance equation in the stop mode is:

$$c_\theta(\omega, i_{CVT}) \cdot \theta + c_i(\omega) \cdot I_c = 0 \quad (3.7)$$

With this in mind, the objective is to find the relations that characterize the operation of the both machines for effective charge sustaining operation. Different engine torques can be produced at different operating speeds and throttle settings. By considering the operating limitation of both machines and the slope of the torque balance line on the θI_c -plane, we have:

$$c_\theta(\omega, i_{CVT}) \cdot \theta = -c_i(\omega) \cdot I_c \Rightarrow \frac{I_{min}}{\theta_{WOT}} = -\frac{c_\theta(\omega, i_{CVT})}{c_i(\omega)} \quad (3.8)$$

where c_θ and c_i are generally determined from the characteristic graphs of the engine and the motor respectively. For instance, for the particular vehicle studied in this study (See details in Section 4.1,)

$$\begin{aligned}
c_\theta &= .0096i_{CVT}(-.0005\omega^2i_{CVT}^2 + .4033\omega i_{CVT}) \\
c_i &= \frac{236}{\omega} \quad (\text{for } \omega > 80)
\end{aligned} \tag{3.9}$$

With these particular values in (3.9), solving (3.8) for ω yields $\omega = \frac{303.1800253}{i_{CVT}}$ which produces:

$$\omega_E = \omega \cdot i_{CVT} \Leftrightarrow N_E \simeq 2895 \text{ rpm} \tag{3.10}$$

Note that this value, while relatively high in comparison with idle engine speed of typical vehicles, produces the highest gain in charge current for a unit change in throttle position for the particular vehicle considered in this study.

The remaining problem at this point is to determine the increment of engine torque for the charge operation ($T_{ec,SOC}$) as a function of deviation of the SOC at the given engine speed (2895 rpm in the case of the vehicle considered here for instance.) In order to resolve this problem, a baseline engine torque is defined. This is accomplished by referring to the engine efficiency map for the vehicle, where for instance for the vehicle considered in this study, operating at the given engine speed of 2895 rpm, the baseline engine torque that corresponds to the lowest specific fuel consumption is approximately 75% of the maximum engine torque. Subsequently, the so called torque margin, TMC, is determined in a similar manner as earlier, that is $TMC = T_{e,max} - T_{e,baseline}$ and the following logic is used to characterize the required engine torque increment for charge sustaining operation:

Case 1: Charge operation ($N < 0$)

$$T_{ec,SOC} = \begin{cases} T_{e,baseline} + TMC \cdot (-N) & \text{if } spc \leq N; \\ T_{e,baseline} + TMC & \text{if } N < spc; \end{cases}$$

Case 2: Charge operation over \overline{SOC} ($N \geq 0$)

$$T_{ec,SOC} = \begin{cases} T_{e,baseline} + TMC \cdot (N) & \text{if } N \leq spd; \\ T_{e,baseline} + TMC & \text{if } spd < N; \end{cases} \quad (3.11)$$

Note that spd and spc are user defined parameters as discussed earlier in the case of hybrid operation.

As shown in (3.11), if the charge operation in the stop mode is requested, charge operation can be performed regardless of “ $N \geq 0$ ” to keep the SOC up to the upper limit for the next use. The upper limit for charge sustaining operation in the stop mode can be set as the target SOC to sustain the SOC at the target SOC level.

3.4.3.4 Vehicle Mode-Based Charge Operation in Hybrid Mode

In order to implement the idea of battery charge operation in the hybrid mode, the following rule set is proposed to adjust the degree of charge operation according to the vehicle’s mode of operation (See rule set in Table 3.14.) The increment of engine torque ($T_{ec,SOC}$) for the charge operation is adjusted by the value of β_{hybrid} ,

$$T_{ec,SOC,hybrid} = \beta_{hybrid} \times T_{ec,SOC} \quad (3.12)$$

Here, β_{hybrid} is the output of a mode-based fuzzy inference system that is driven by the operating mode of the vehicle and generates a weighted value of $[0 \sim 1]$ representing the degree of charge according to the vehicle modes. For instance, if the vehicle experiences high acceleration, additional battery charge is prohibited to avoid deteriorating the vehicle’s performance even in low level of the SOC in the battery.

The value of β_{hybrid} is set to zero ($\beta_{hybrid} = “Z,”$) whenever the level of the SOC is high in all modes. In the cruise and deceleration mode, battery charge operation is performed according to the engine speed under low SOC level. In the acceleration mode, battery charge operation is dependent on the magnitude of power demand under low SOC level.

Table 3.14 Rule set for mode-based charge operation in the hybrid mode

Vehicle mode	T_{dc}	N_E	SOC	β_{hybrid}
Acceleration	PS	L	H	Z
	PB	L	H	Z
	PS	H	H	Z
	PB	H	H	Z
	PS	L	L	L
	PB	L	L	S
	PS	H	L	L
	PB	H	L	S
Cruise	Z	L	H	Z
	Z	H	H	Z
	Z	L	L	S
	Z	H	L	L
Deceleration	N	L	H	Z
	N	H	H	Z
	N	L	L	S
	N	H	L	L

Note: N, Negative; Z, Zero; L, Low; S, Small; H, High; PS, Positive Small; PB, Positive Big.

Again, from (3.12), torque balance equation in (3.3), is modified as follows:

$$T_e + \underbrace{T_{ec,FTD} \times (1 + \overbrace{\text{sgn}(T_{ec,FTD}) \cdot \alpha_{DSI}}^{\text{propulsion}})}_{\text{Engine}} + \underbrace{T_{ec,SOC} \times \beta_{hybrid}}_{\text{charging}} + \underbrace{T_{mc}}_{\text{Motor}} = T_c \quad (3.13)$$

Membership functions used in the mode-based charge operation are shown in Fig. 3.10 for input variables, and in Fig. 3.17 for output variable.

3.5 Conclusion

In this chapter, a concept for a “driving situation awareness”-based intelligent energy management system for parallel hybrid electric vehicles has been presented. This

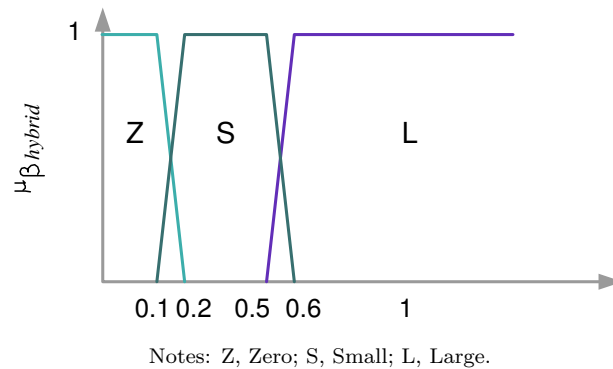


Figure 3.17 Membership function of output variable in mode-based charge operation

concept is based on the idea that fuel mileage and pollutant emissions are a direct consequence of driving in a driving environment that influences the operation of the vehicle. To implement this idea in a system that coordinates the functioning of power sources in the powertrain, an intelligent energy management system was devised. The main task in this study was to design the proposed energy management agent following the design of each sub agent (or subsystem) that performs the missions assigned to it. This work also includes the efforts on examining the factors that characterize its mission. In summary, the proposed intelligent energy management agent incorporates the following subsystems:

- Driving Information Extractor (DIE)
- Driving SIuation Identifier (DSII)
 - Roadway Type Identifier (RTI)
 - Driving Trend Identifier (DTI)
 - Driving Mode identifier (DMI)
 - Driving Style Identifier (DSI)
- Fuzzy Torque Distributor (FTD)
- State-of-Charge Compensator (SCC)

CHAPTER IV

SIMULATION STUDY

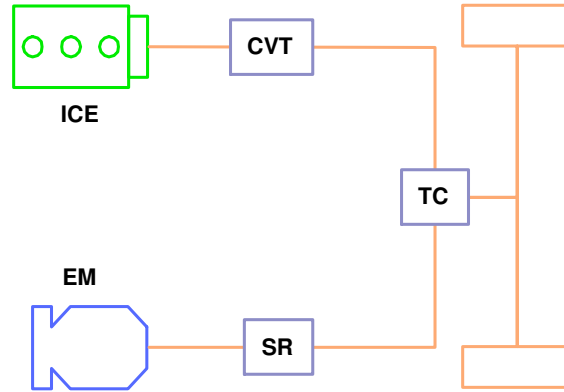
In this chapter, I present the simulation study to evaluate the proposed energy management system. Computational simulation works were performed on the facility-specific drive cycles [35] and the EPA Urban Dynamometer Driving Schedule (UDDS) [48]. For the simulation, a typical parallel hybrid drivetrain was constructed. Simulation factors affecting the performance of the subsystems in IEMA are addressed. Analysis of simulation results is performed in details.

4.1 Hybrid Vehicle Configuration

For the simulation study, a typical parallel drivetrain with the continuous variable transmission (CVT) is used. The mathematical models of the power train components are taken from [49]. The vehicle has a total mass of 1655 kg which is the sum of the curb weight of 1467 kg and the battery weight. An internal combustion engine with a displacement of 0.77 L and peak power of 25 kW is chosen. The electric motor is chosen to meet the acceleration performance (zero to 60 mph in less than 15 sec.) In order to satisfy the requirement for acceleration, a motor with a power of 45 kW is selected. The battery capacity is 6 kW·h (21.6 MJ) with a weight of 188 kg and is chosen on the basis of estimated values of the lead acid battery type used in a conventional car. Typical parallel drivetrain with the CVT is shown in Fig 4.1.

4.2 Simulation Factors Affecting Performance of IEMA

The performance of IEMA is affected by the parameters defined at each subsystem, such as the sizes of time windows of long and short term past driving history (T_{lt} and T_{st}), information update period (T_{iu}), and initial roadway type (IRT) setting (See



Note: ICE, Internal combustion engine; EM, Electric motor; CVT, Continuously variable transmission; SR, Speed reducer; TC, Torque combiner.

Figure 4.1 Parallel hybrid drivetrain configuration

Fig. 4.2) as well as torque distribution and charge sustenance strategies proposed in this study.

The data in the interval T_{lt} is used for the identification task of roadway type and driving style of the driver in RTI and DSI, respectively. The proper setting of the length of T_{lt} is necessary for RTI and DSI. If the length of the time window is too short, the performance of RTI and DSI will be more sensitive to the driving variability, resulting in misclassification of roadway type and/or the driver's behavior. It is shown from [38] that in city driving, one cycle of driving from stop, through driving to the next stop may be done within three or four minutes, when considering the frequency of stop and other traffic conditions. For the driving trend recognition, driving data in the range of T_{st} are used in DTI. Again, the choice of the length of T_{st} affects the performance of the vehicle, since driving trend is changed rapidly, and the resulting driving trend recognition is sensitive to the length of time selected. The term T_{iu} is used to indicate when the roadway type and driving style are updated periodically in IEMA.

Note that during the first T_{lt} of driving, neither RTI nor DSI is activated, since driving data is not sufficient to extract a rich set of driving information. For this region, a facility type is initially set, and the driving style is set as *normal* for IEMA

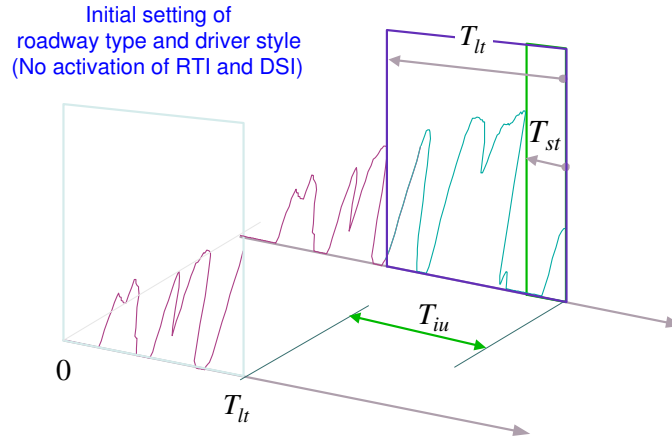


Figure 4.2 Simulation factors

to operate properly.

4.3 Evaluation on the Facility-Specific Drive Cycles

Simulation study on the facility-specific drive cycles enable us to evaluate the performance of IEMA directly, since fuzzy rule sets have been developed based on the characteristics of each of the nine facility-specific drive cycles [35] considered in this study, and adopted as a knowledge base in the fuzzy torque distributor.

As a baseline setting, a typical simulation parameters of $[T_{lt}, T_{st}, T_{iu}]$ were set as $[150, 10, 10]$ sec. For the charging operation in the battery, nominal level of the SOC (target SOC) is typically set as 50% with the normal HEV operating range that would be about 20% either side of the nominal level.

Simulation works were performed for the nine facility-specific drive cycles under the above baseline simulation setting. For each drive cycle, different initial roadway types were set to show their effects on the performance of the vehicle. As mentioned earlier, for the first T_{lt} of driving, no activation of DSI and RTI is made due to insufficient driving data. Instead, driving style of the driver is initially set as *normal*, and the initial roadway type (IRT) is selected as if the vehicle starts driving on the

roadway that is selected initially. One important thing to be noticed is that when RTI is OFF, a single fixed fuzzy rule base that forms a pair with the initial roadway type is activated and governs the flow of energy in the powertrain throughout the driving.

When RTI is ON, first the setting of the initial roadway type is used to select the fuzzy rule base for the first T_{lt} of driving. Subsequently, RTI performs the roadway type identification task periodically (at every T_{iu}) and feeds the roadway type information into FTD. Depending on the roadway type information, a fuzzy rule base that parallels the given roadway type is activated.

4.3.1 Effect of Roadway Type Identifier (RTI)

The effect of the roadway type identifier (RTI) on the overall performance (in terms of *energy usage*¹) for the driving on the facility-specific drive cycles is presented.

In the fuzzy torque distributor, information about roadway type is used to index a fuzzy rule base paralleling to the given roadway type. Again, the usage of the initial roadway type is to initialize a roadway type for the first T_{lt} of driving (due to insufficient data for identification), and/or to index a fuzzy rule base paralleling the initial roadway type itself.

The following are the evaluation criteria for the effect of RTI on the facility-specific drive cycles.

1. If the initial roadway type (IRT) is set as the same type as the actual roadway type (RT, actual drive cycle at hand), then we expect

$$Performance_{RTI=ON} \lesssim Performance_{RTI=OFF} \quad \text{under IRT} = \text{RT},$$

¹Energy usage in this study is the integration of the overall energy consumption rate (both fuel and battery energy) with respect to time. The computation of energy usage is made by introducing an *equivalent energy consumption rate* (EECR) for fuel usage. The fuel flow rate of the engine is translated into an equivalent amount of the energy consumption rate of a battery by multiplying the fuel flow rate by the specific energy of fuel: $EECR = \text{fuel flow rate [g/sec]} \times \text{specific energy of fuel [Joule/g]}$. Here, specific energy of fuel is the amount of energy (heat) released in the burning of fuel. With the EECR and the energy consumption rate in the battery, the overall energy consumption rate can be calculated.

since it is believed under $IRT = RT$ that the following situation would occur: When RTI is OFF, a single fixed, roadway-type based fuzzy rule base paralleling IRT (again, paralleling RT), is activated for the driving on the actual drive cycle. Thus, the possibility of misclassification of the roadway type from RTI can be excluded.

2. If the initial roadway type (IRT) is set as different one as the actual roadway type (RT), then we expect

$$Performance_{RTI=ON} \gtrsim Performance_{RTI=OFF} \text{ under } IRT \neq RT$$

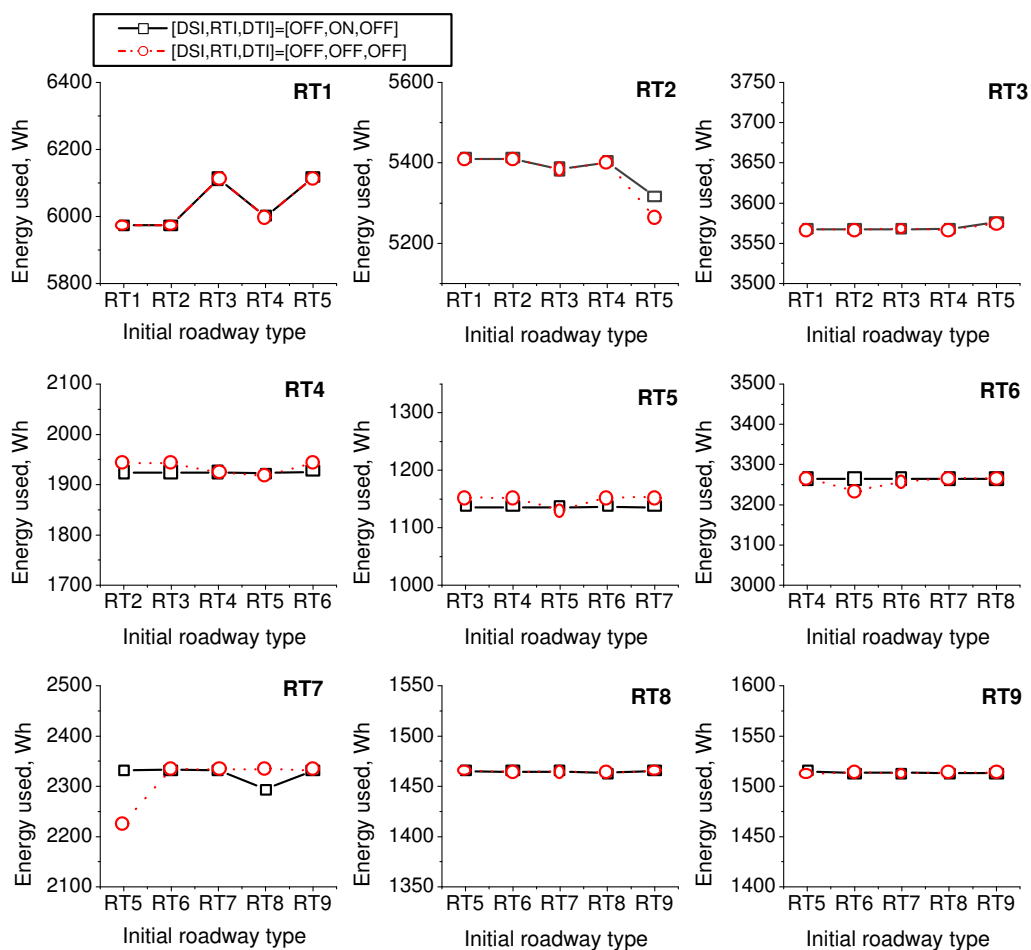
Regarding this, we believe that when RTI is ON, a fuzzy rule base matching with the actual drive cycle is activated with the aid of RTI, although, the fuzzy rule base paralleling IRT is misused in the first T_{lt} of driving.

4.3.1.1 Effect of RTI under $[DSI,DTI]=[OFF,OFF]$

When the driving trend information is not available ($DTI = [OFF]$) in the fuzzy rule base of FTD, fuzzy rule set being indexed only by driving mode recognition are activated and fired. Simulation results, as shown in Fig. 4.3, reveal that single effect of RTI on energy consumption along with the initial roadway types is minute over nine drive cycles. Although no significant improvement is shown, overall trend of energy-usage pattern meets our expectation described in evaluation criteria.

4.3.1.2 Effect of RTI under $[DSI,DTI]=[ON,ON]$

In this case, it is not easy to separate the single effect of RTI on performance from the overall performance with the activation of DSI and DTI. From the simulation result shown in Fig. 4.4, when the case of $IRT = RT$, the overall trend of energy usage over the drive cycles meets the performance criteria: $Performance_{RTI=ON} \lesssim Performance_{RTI=OFF}$ under $IRT = RT$. On the other hand, when $IRT \neq RT$, it does not follow the performance criteria, while it seems that the overall performance is the output blended with the effect of DSI and DTI, as well as RTI. Simulation results,



Note: RT1, High-speed freeway; RT2, Freeway under LOS A-C; RT3, Freeway under LOS D; RT4, Freeway under LOS E; RT5, Freeway under LOS F; RT6, Arterial/Collector under LOS A-B; RT7, Arterial/Collector under C-D; RT8, Arterial/Collector under E-F; RT9, Local roadway.

Figure 4.3 Effect of RTI under [DSI,DTI]=[OFF,OFF]

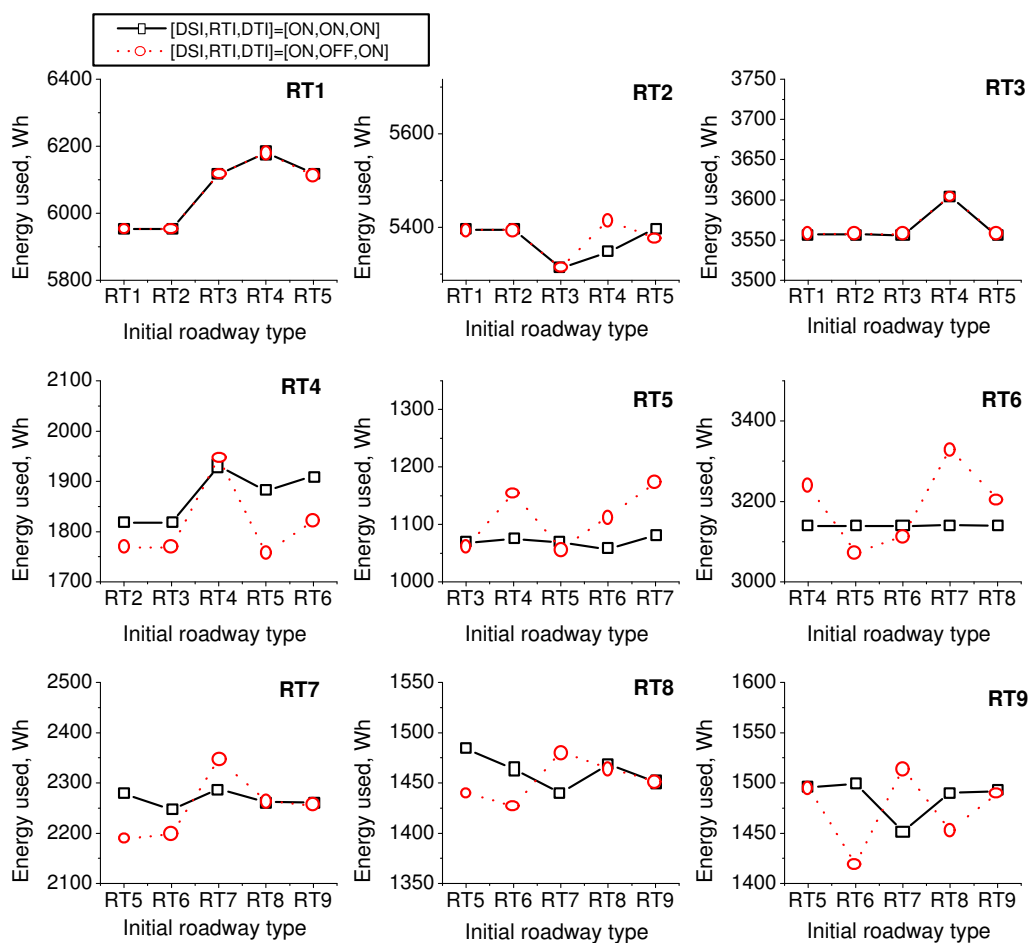
however, shows a more steady pattern in energy usage on the average under $[DSI, DTI]=[ON,ON]$ over nine drive cycles.

4.3.2 Effect of $[DSI,DTI]$ under $RTI=[ON]/[OFF]$

Simulation results shown in Figs. 4.5 and 4.6 reveal that the overall trend of energy usage due to the effect of $[DSI,DTI]$ along with the initial roadway type setting is promising for each (facility-specific) drive cycle, regardless of the activation status of RTI. This implies that the consideration of the effect of driving trend as well as driving style improves the overall performance.

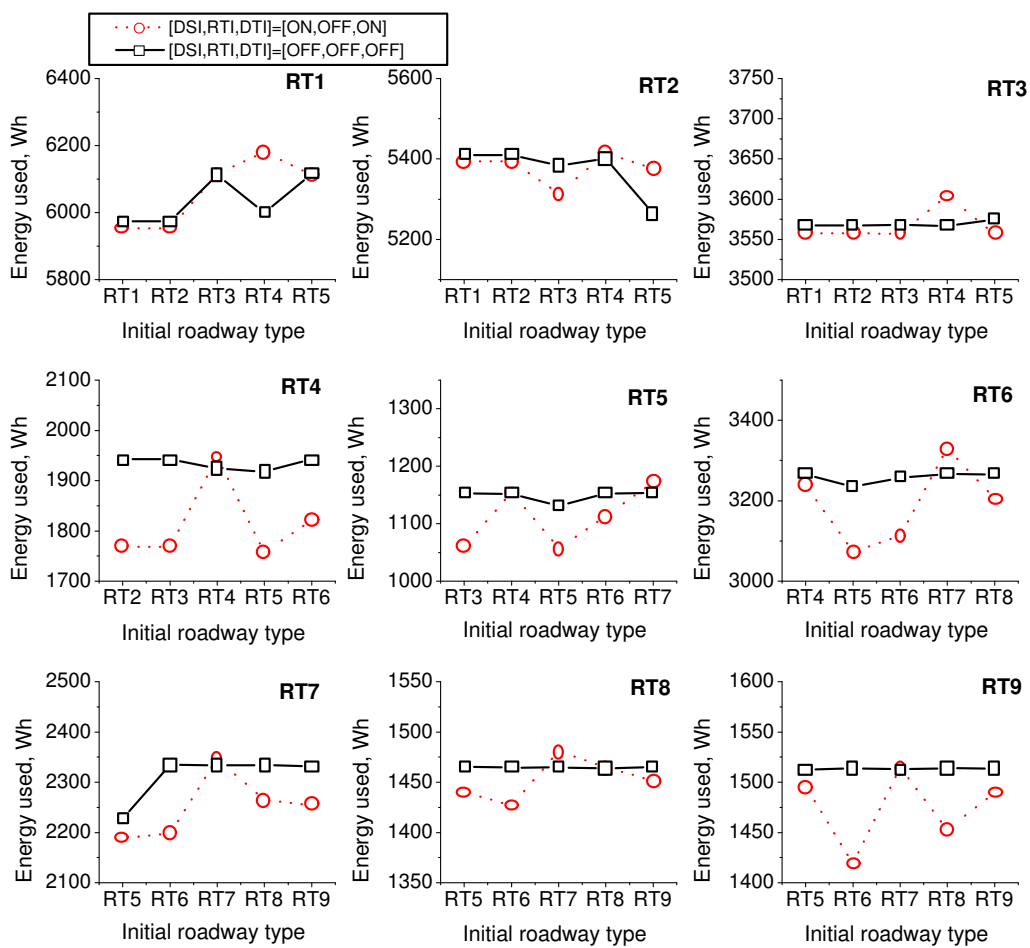
4.3.3 Effect of $[DSI,DTI]$ versus RTI

The results of the comparison of the single effect of $[DSI,DTI]$ with RTI can be understood as follows. As mentioned earlier, the identification of the roadway type is made using long-term driving data, implying that the variability in the roadway type changes has less influence on the operation of the vehicle (than that of driving trend), consequently affecting the fuel consumption (and emissions) less. On the other hand, driving trend (i.e., modal transition of the vehicle) is identified with short-term driving data compared with the roadway type identification, since driving trend of the vehicle can change rapidly. In general, fuel consumption is a direct consequence of how the engine is effectively used, and is closely related to the operating pattern (mode) of the vehicle. Since fuel consumption is sensitive to the variation of modes of operation of the vehicle, use of driving trend information (as well as driving style) for coordinating energy flow in the drivetrain would eventually improve the overall performance compared with use of information on the roadway type alone. It can be seen from the simulation results that in most cases of driving, the effect of $[DTI,DSI]$ is dominant over that of RTI alone, as I expected (See Fig. 4.7.)



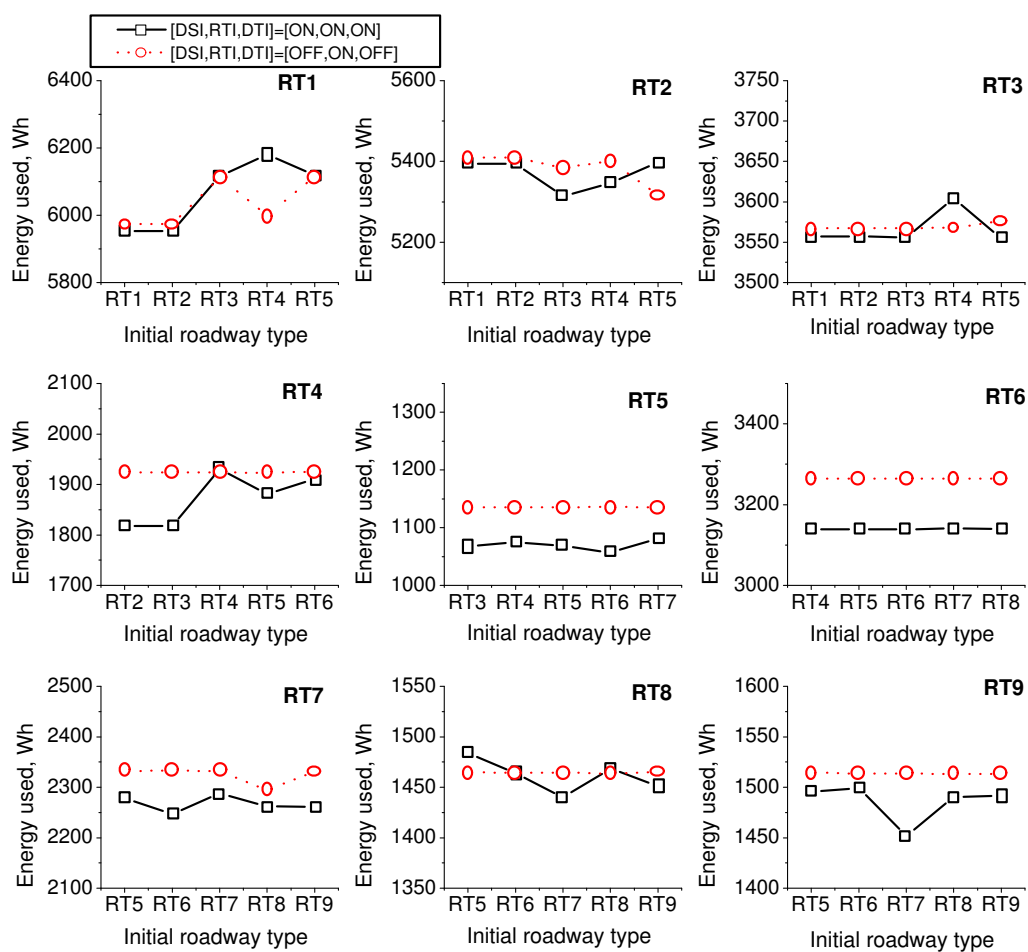
Note: RT1, High-speed freeway; RT2, Freeway under LOS A-C; RT3, Freeway under LOS D; RT4, Freeway under LOS E; RT5, Freeway under LOS F; RT6, Arterial/Collector under LOS A-B; RT7, Arterial/Collector under C-D; RT8, Arterial/Collector under E-F; RT9, Local roadway.

Figure 4.4 Effect of RTI under [DSI,DTI]=[ON,ON]



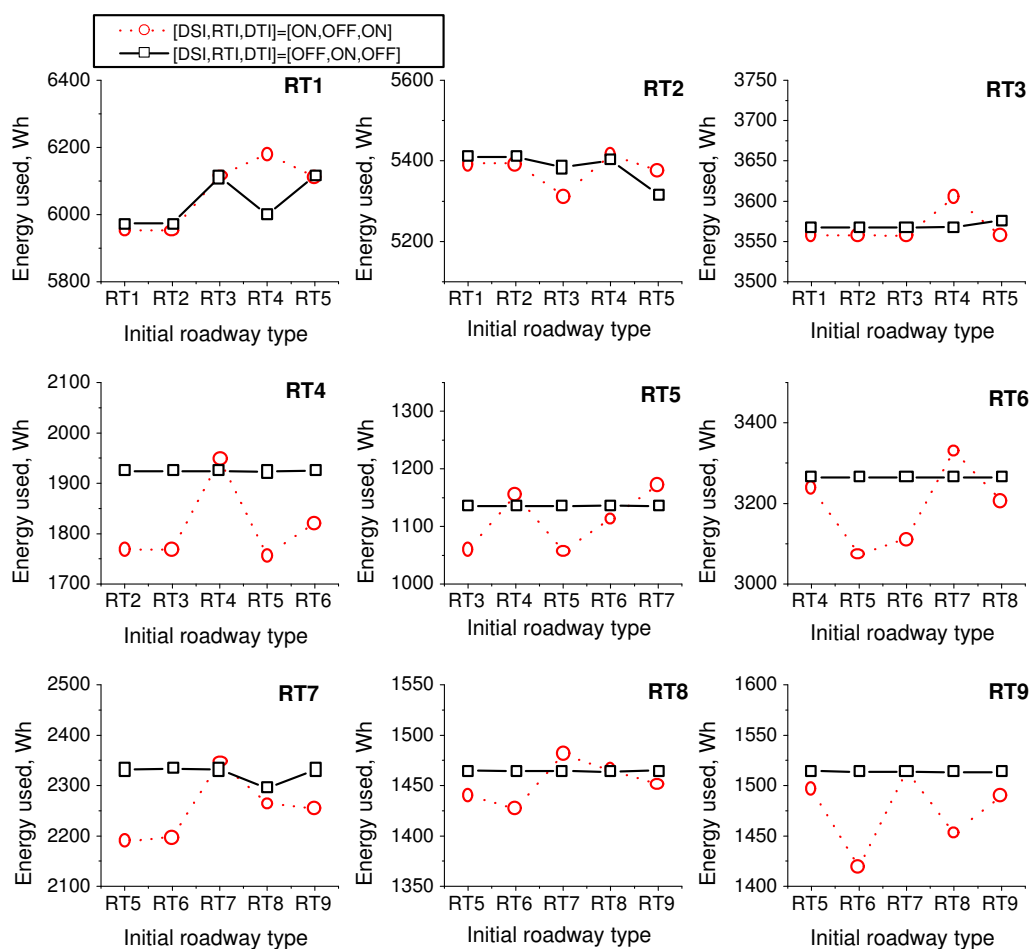
Note: RT1, High-speed freeway; RT2, Freeway under LOS A-C; RT3, Freeway under LOS D; RT4, Freeway under LOS E; RT5, Freeway under LOS F; RT6, Arterial/Collector under LOS A-B; RT7, Arterial/Collector under C-D; RT8, Arterial/Collector under E-F; RT9, Local roadway.

Figure 4.5 Effect of [DSI,DTI] under RTI=[OFF]



Note: RT1, High-speed freeway; RT2, Freeway under LOS A-C; RT3, Freeway under LOS D; RT4, Freeway under LOS E; RT5, Freeway under LOS F; RT6, Arterial/Collector under LOS A-B; RT7, Arterial/Collector under C-D; RT8, Arterial/Collector under E-F; RT9, Local roadway.

Figure 4.6 Effect of [DSI,DTI] under RTI=[ON]



Note: RT1, High-speed freeway; RT2, Freeway under LOS A-C; RT3, Freeway under LOS D; RT4, Freeway under LOS E; RT5, Freeway under LOS F; RT6, Arterial/Collector under LOS A-B; RT7, Arterial/Collector under C-D; RT8, Arterial/Collector under E-F; RT9, Local roadway.

Figure 4.7 Effect of [DSI,DTI] versus RTI

4.3.4 Overall Effect of Subsystems

It is shown from Fig. 4.8 that the overall performance with full activation of subsystems is higher over the nine drive cycles than that with partial activation of subsystems, as I expected.

In conclusion, the overall performance was compared with each other in terms of energy used, since it is not easy to calculate the effective fuel mileage considering the fuel usage to charge the battery as well as to propel the vehicle. Although it is not easy to distinguish the individual effects of subsystems, simulation results reveal that the overall performance can be improved under the supervision of IEMA as an onboard intelligence for energy management of parallel hybrid vehicles.

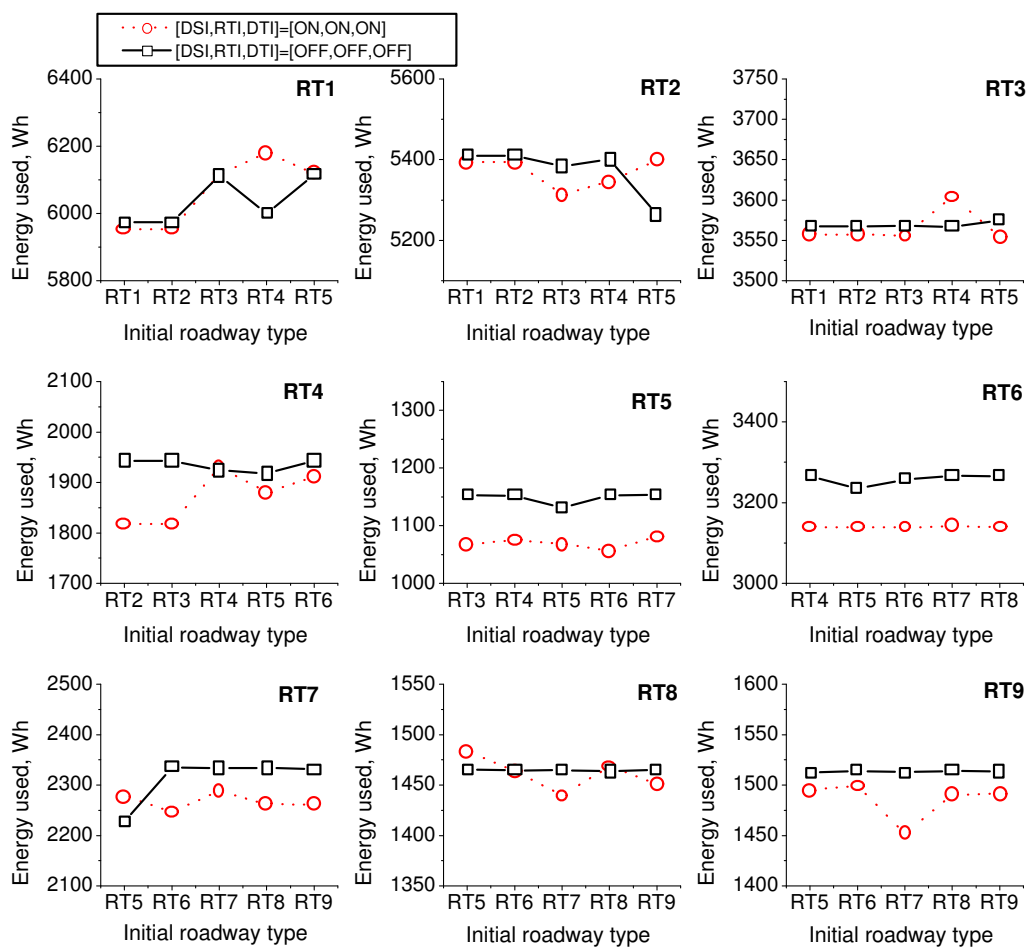
4.4 Evaluation on the Urban Dynamometer Driving Schedule

In this section, the performance of the vehicle under the supervision of IEMA on the UDDS is investigated. Simulation works were performed with different settings of the initial roadway types, time factors T_{lt} (for DSI and RTI) and T_{st} (for DTI,) and (de)activation of the subsystems. Evaluation of IEMA is accomplished through the understanding of the effects on the performance of subsystems, time factor setting and initial roadway type setting.

4.4.1 Effect of Subsystems

The EPA urban dynamometer driving schedule (UDDS) was developed to represent light-duty vehicle operation under urban driving conditions characterized as ones over a relatively long route that traverses numerous roadway links and a variety of roadway types, ranging from two-lane surface streets to multi-lane freeways [50] (See Fig. 4.9.)

My preliminary simulation study on the UDDS indicates that the UDDS is a composite cycle that can be decomposed into different types of roadway. For instance, especially in this simulation, the UDDS is decomposed into the facility-specific drive cycles considered in this study as shown in Fig. 4.10. The percentage values on



Note: RT1, High-speed freeway; RT2, Freeway under LOS A-C; RT3, Freeway under LOS D; RT4, Freeway under LOS E; RT5, Freeway under LOS F; RT6, Arterial/Collector under LOS A-B; RT7, Arterial/Collector under C-D; RT8, Arterial/Collector under E-F; RT9, Local roadway.

Figure 4.8 Overall effect of subsystems

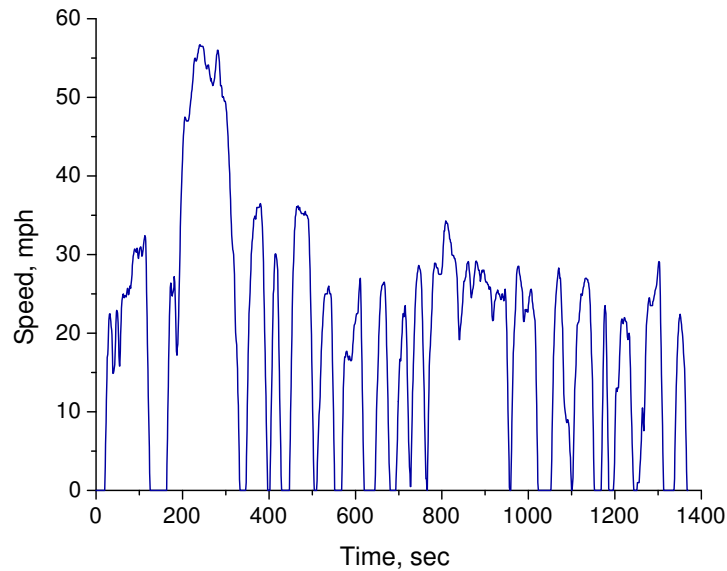


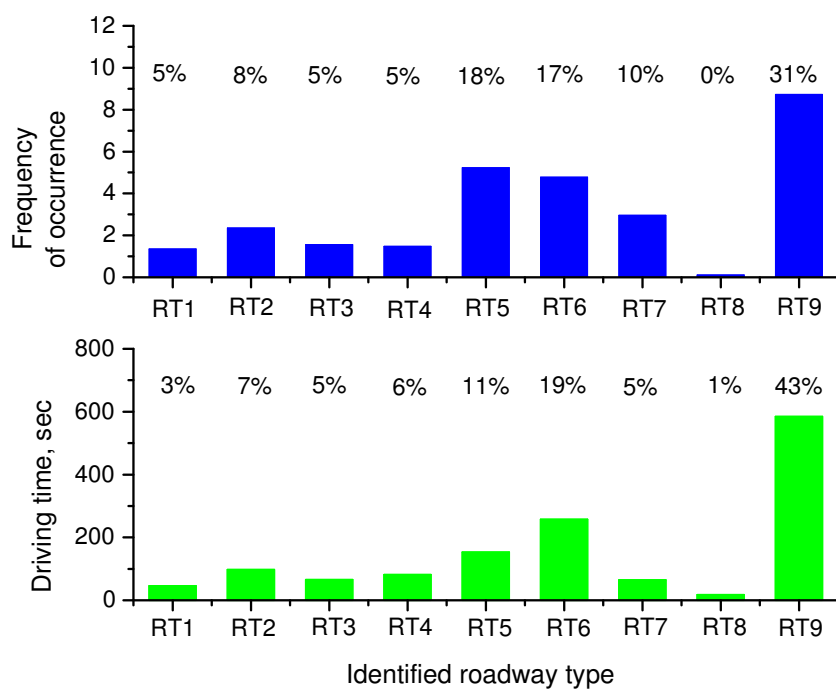
Figure 4.9 EPA Urban dynamometer driving schedule

the figure are average ones from the simulation results with different setting of time factors and initial roadway types.

Since the UDDS consists of a variety of roadway types that conceivably show different types of driving style and vehicle operation, the performance of the vehicle, in this simulation, is the consequence of the blended output generated in IEMA activated by the identified roadway type information, the driving trend and the mode of operation of the vehicle under a specific driving situation being identified. Thus individual analysis of each subsystem in IEMA is not a trivial task. However, the prediction and understanding of the expected trend (impact) of each subsystem enables us to evaluate the effect of IEMA on the overall performance.

4.4.1.1 Effect of RTI

In the main, it is expected that the activation of RTI would give better performance. However, I suspect that the overall performance on the UDDS would vary depending



Note: RT1, High-speed freeway; RT2, Freeway under LOS A-C; RT3, Freeway under LOS D; RT4, Freeway under LOS E; RT5, Freeway under LOS F; RT6, Arterial/Collector under LOS A-B; RT7, Arterial/Collector under C-D; RT8, Arterial/Collector under E-F; RT9, Local roadway.

Figure 4.10 Decomposition of UDDS through roadway type identification

on the initial roadway type setting and the actually identified roadway type of the UDDS. The selection of the initial roadway type affect the operation of FTD according to the status of activation of RTI. When the roadway type identifier is functioning (i.e., $RTI = [ON]$), for the first T_{lt} of driving, FTD is forcibly commanded to operate following the initial roadway type setting. Thus, as far as the actual roadway type of the UDDS for the first T_{lt} is similar (or equal) to the initial roadway type, improved performance can be expected. Again, when the roadway type identifier is deactivated (i.e., $RTI = [OFF]$), the operation of FTD is driven absolutely according to the initial roadway type throughout driving. In this case, the improvement of performance is expected only when the actual roadway type on the UDDS has more portion that is identical to the initial roadway type (such as the case that the local roadway cycle (RT9) is set as the initial roadway type under $RTI = [OFF]$, as shown in Fig. 4.10.) Therefore, the overall performance without activation of RTI would be better in some cases. Since the UDDS is a composite cycle and the overall performance is the consequence of the blended output of IEMA accordingly, it is not easy to say which portion of the effect is from RTI.

4.4.1.2 Effect of [DSI,DTI]

As described in Section 4.3.2, a modal transition (e.g., change from acceleration to cruise mode) of the vehicle during driving over a specific driving situation would directly impact on fuel consumption and exhaust gas emissions. In this study, the effect of modal transition is incorporated in FTD, which is designated by the driving trend. From this architecture in FTD, I expect that the overall performance would be improved with the information of driving trend as well as driving mode of operation of the vehicle.

4.4.2 Effect of Initial Roadway Type

As described before, the effect of initial roadway type setting on the performance is directly coupled with the operation of FTD (specifically, fuzzy rule base paralleling

the roadway type set initially.) The performance resulting from the setting of the initial roadway type varies depending on the activation status of RTI.

4.4.2.1 *RTI=[OFF]*

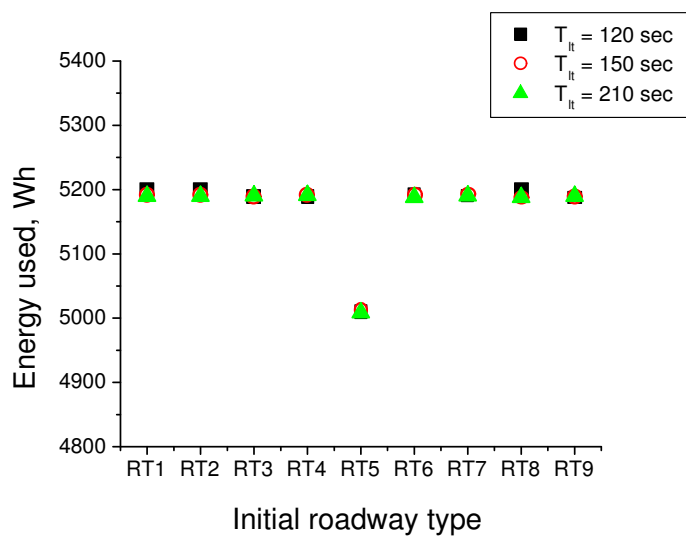
When the roadway type identifier is disabled, the selection of the initial roadway type determines the overall performance of the vehicle throughout driving; a fixed rule base corresponding to the initial roadway type is used. Simulation results shown in Fig. 4.11 reveal the following:

1. When both DSI and DTI are deactivated, no big differences in performance is found along with the initial roadway type settings except for the case of IRT = RT5.
2. When both DSI and DTI are activated, the effects of the different settings of the initial roadway type are observed. The performance variation at each IRT setting may be from the effects of DSI (with different T_{lt} 's) and DTI (in this case, $T_{st} = 10$ sec.)

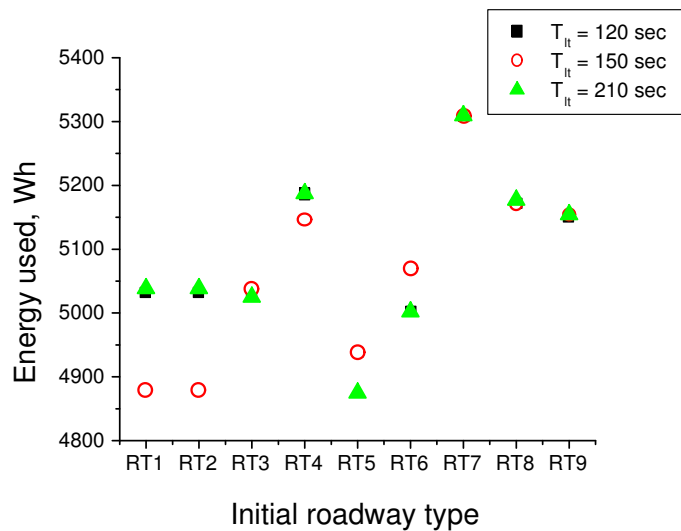
Again, a similar trend is observed at $T_{st} = 15$ sec with different T_{lt} 's, which affects the driving trend identification (See Fig. 4.12.)

4.4.2.2 *RTI=[ON]*

When the roadway type identifier is enabled, the initial roadway type setting has an influence on the performance during the first T_{lt} of driving from start (i.e., one of the fuzzy rule bases in FTD is initiated by the initially set roadway type for the time of T_{lt} .) After passing the first T_{lt} , the overall performance is affected by the identified roadway type from RTI. If the initial roadway type is set as the roadway type that would show the same type as one on the UDDS, the performance during this time would be improved. Figures 4.13 and 4.14 are the simulation results that show the effect of RTI along with initial roadway type settings. Similar to the previous case, no big differences in performance was found along with the initial roadway type setting



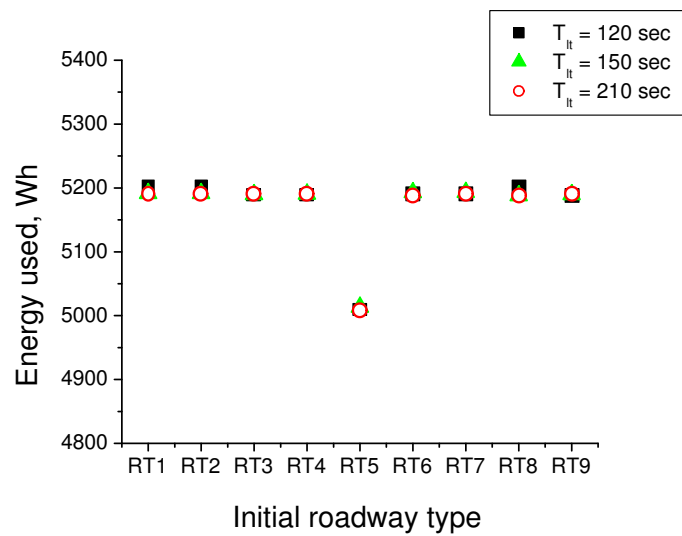
(a) [DSI,RTI,DTI] = [OFF,OFF,OFF]



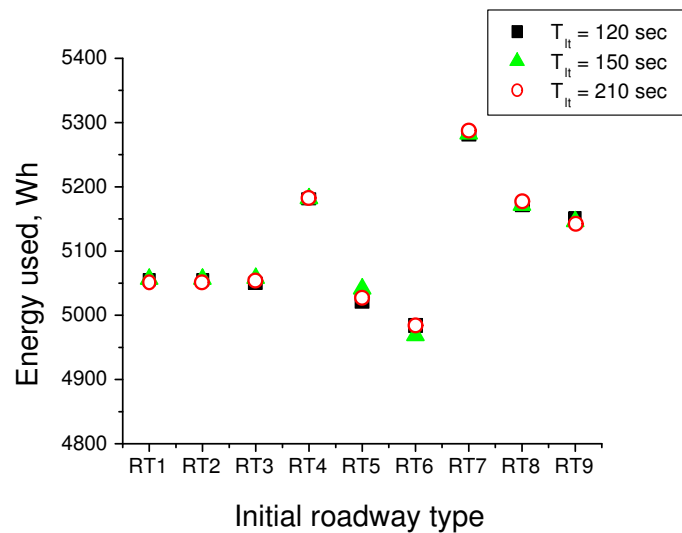
(b) [DSI,RTI,DTI] = [ON,OFF,ON]

Note: RT1, High-speed freeway; RT2, Freeway under LOS A-C; RT3, Freeway under LOS D; RT4, Freeway under LOS E; RT5, Freeway under LOS F; RT6, Arterial/Collector under LOS A-B; RT7, Arterial/Collector under C-D; RT8, Arterial/Collector under E-F; RT9, Local roadway.

Figure 4.11 Effect of IRT when RTI is off; $T_{st} = 10$ sec (for $T_{iu} = 10$ sec)



(a) [DSI, RTI, DTI] = [OFF, OFF, OFF]



(b) [DSI, RTI, DTI] = [ON, OFF, ON]

Note: RT1, High-speed freeway; RT2, Freeway under LOS A-C; RT3, Freeway under LOS D; RT4, Freeway under LOS E; RT5, Freeway under LOS F; RT6, Arterial/Collector under LOS A-B; RT7, Arterial/Collector under C-D; RT8, Arterial/Collector under E-F; RT9, Local roadway.

Figure 4.12 Effect of IRT when RTI is off; $T_{st} = 15$ sec (for $T_{iu} = 10$ sec)

when both DSI and DTI are deactivated. On the other hand, when both DSI and DTI are activated, it is observed that the overall performance is improved on the average and the performance difference at each initial roadway type setting for different time settings is distinguishable.

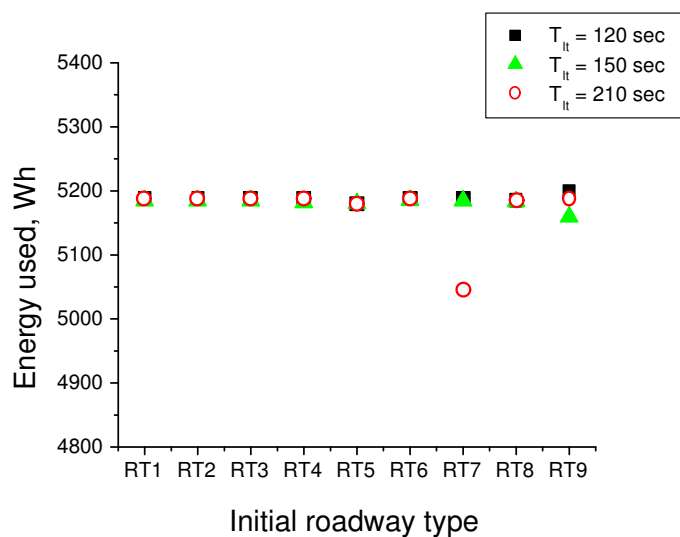
4.4.3 Effect of Time Setting

The size of T_{lt} impacts the performance of RTI and DSI, while the size of T_{st} affects DTI on the performance. As stated earlier, identification of the roadway type needs proper choice of the time span T_{lt} . For the identification of the roadway type combined with the level of traffic congestion, relatively large size of the driving data is need to allow RTI to cover all spectrum of variability of driving situation. Again, the effect of the size of the driving data ($=T_{lt}$) on driver style identification can be explained in the same way as of RTI. Since the UDDS is a composite cycle, direct observation of this effect is not available. In general, however, we can see from the simulation results that energy usages were reduced for large T_{lt} . This effect is more distinguishable under the activation of DSI and DTI (See Figures 4.13 and 4.14.)

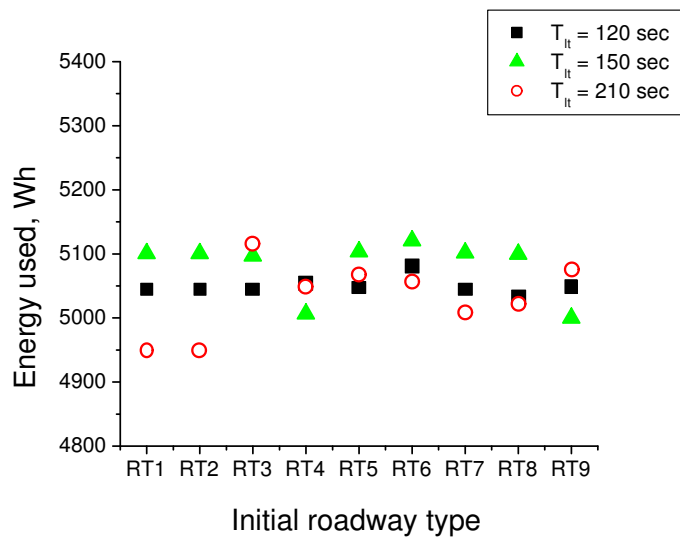
The effect of T_{st} can be understood as follows: since driving trend, which is meant by a modal transition (e.g., acceleration to cruise mode in operation of the vehicle,) can be changed rapidly, taking a large time span of T_{st} for the identification of driving trend may cause DTI to make wrong recognition on the driving trend that the vehicle is experiencing. This may dilute the variability in vehicle's operating mode changes and fail to recognize the vehicle operation properly, resulting in deterioration of the overall performance. As shown in Figures 4.13 and 4.14 (b), we can see that for $T_{st} = 15$ sec, more energy was used for driving on the UDDS on the average.

Not presented here, we observe from the simulation study that it is not easy to describe the effect of the information update time T_{iu} , and is dependent on the real driving situation. However, we know that the proper choice of T_{iu} is necessary to improve the overall performance of the vehicle and should be selected in an adaptive manner as well as T_{lt} and T_{st} .

Figure 4.15 contains the time history data of simulation results representing



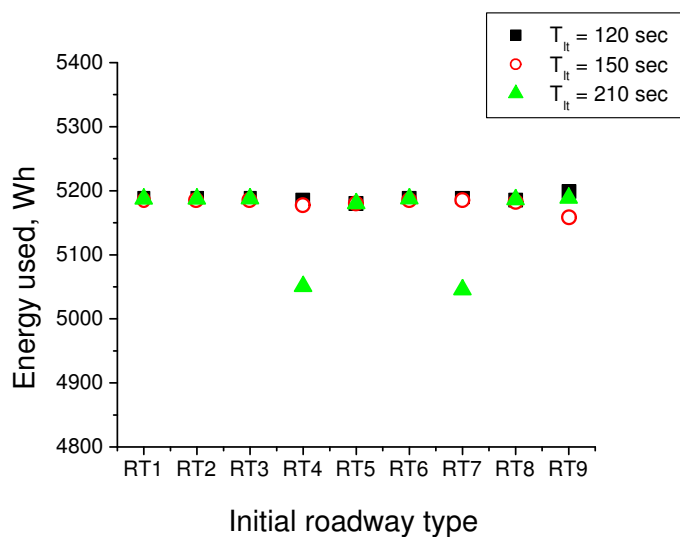
(a) [DSI,RTI,DTI] = [OFF,ON,OFF]



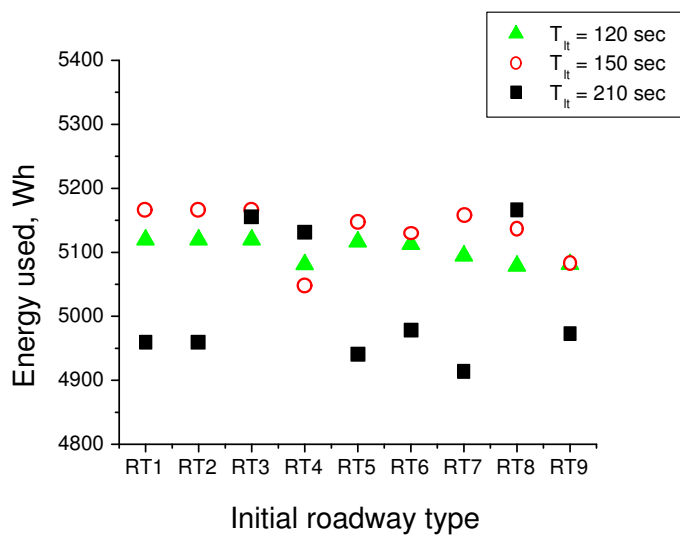
(b) [DSI,RTI,DTI] = [ON,ON,ON]

Note: RT1, High-speed freeway; RT2, Freeway under LOS A-C; RT3, Freeway under LOS D; RT4, Freeway under LOS E; RT5, Freeway under LOS F; RT6, Arterial/Collector under LOS A-B; RT7, Arterial/Collector under C-D; RT8, Arterial/Collector under E-F; RT9, Local roadway.

Figure 4.13 Effect of IRT when RTI is on; $T_{st} = 10$ sec (for $T_{iu}=10$ sec)



(a) [DSI,RTI,DTI] = [OFF,ON,OFF]



(b) [DSI,RTI,DTI] = [ON,ON,ON]

Note: RT1, High-speed freeway; RT2, Freeway under LOS A-C; RT3, Freeway under LOS D; RT4, Freeway under LOS E; RT5, Freeway under LOS F; RT6, Arterial/Collector under LOS A-B; RT7, Arterial/Collector under C-D; RT8, Arterial/Collector under E-F; RT9, Local roadway.

Figure 4.14 Effect of IRT when RTI is on; $T_{st} = 15$ sec (for $T_{iu} = 10$ sec)

the behaviors of the subsystems (driving style identifier, roadway type identifier, and fuzzy torque distributor) and components (engine, motor, and battery) on the UDDS.

4.4.4 *Comments on Roadway Type Identification*

One important feature to be noticed here on the roadway type identifier is its ability to transform the whole drive cycle into a set of basis drive cycles, each of which has its own traffic situation (facility-specific) characteristics in terms of roadway type and level of congestion. By applying the roadway type identification process to a drive cycle, one can obtain a further information from the drive cycle that is not readily available in the drive cycle itself. This information may be helpful in the fuel economy test for driving on the drive cycle to be analyzed. In addition, for the purpose of development of drive cycles one can take advantage of transformation with roadway type identification process.

4.5 Conclusions

Computational simulations were performed to evaluate proposed IEMA system for a parallel hybrid vehicle on the facility-specific drive cycles [35] and the EPA Urban Dynamometer Driving Schedule (UDDS) [48]. Simulation results were reported and analyzed to ensure the viability of proposed energy management system. The performance analysis proves that the proposed traffic situation awareness-based energy management system can enhance overall performance. The major improvement of vehicle performance can be reached by considering the driving environment, especially roadway type in connection with the level of traffic congestion, driving style of the driver, and the vehicle's operating mode and its trend of modal change. One thing to be considered more carefully in the design of the proposed system is the selection of the time factors (T_{lt} , T_{st} and T_{iu}) in subsystems which affects performance of the vehicle. It is recommended that those factors should be selected adaptively for economic driving on an arbitrary driving environment. Adding this capability to the

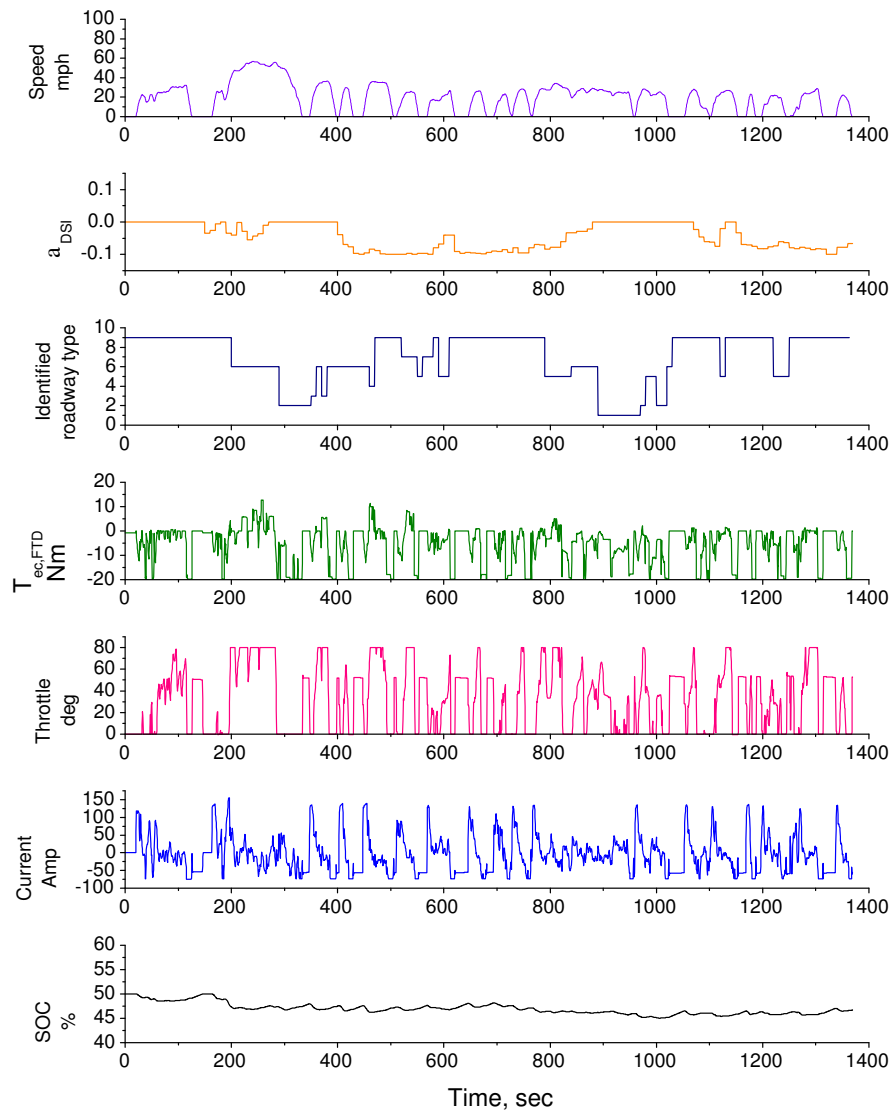


Figure 4.15 Performance results on the UDDS: $[T_{lt}, T_{st}, T_{iu}] = [150, 10, 10]$ sec; IRT = RT9; $[DSI, RTI, DTI] = [ON, ON, ON]$

energy management system would result in a better overall vehicle control design.

CHAPTER V

CONCLUSION

Hybrid electric vehicles represent an emerging technology, but many efforts are still to be developed to put valuable product on the market. The demand of research and development, and design effort in the field of drives, energy sources and energy management control is becoming enormous and a challenging field in the US. The purpose of this study was the design of an intelligent energy management control for parallel hybrid electric vehicles, which coordinates the energy flow in the drivetrain for enhanced fuel economy (and reduced pollutant emissions.)

Traffic situation awareness based energy management system was proposed and investigated as a possible new energy management system for parallel HEVs. Control strategies for torque distribution and charge sustenance tasks have been developed and implemented in the proposed intelligent energy management system (we referred to as intelligent energy management agent (IEMA).) A computer program was made to evaluate its viability in terms of fuel economy and overall energy usage. The simulation was performed on the Urban Dynamometer Driving Schedule and nine facility-specific drive cycles used in the design of energy management system. The results presented in the simulation study prove that the proposed IEMA provides a possible solution to and an extendable framework of energy management system for parallel HEVs.

There, however, may be some notes to be considered for adding viability to IEMA.

1. Fuzzy rule packages implemented in FTD presents only fuel economy oriented torque distribution strategy (i.e., considering fuel consumption with priority for torque distribution operation given traffic situation.) Even for this purpose, there are a lot of sets of alternatives describing the characteristics of relationship between driving situation and fuel economy. Future work should include the development of sets of emissions-oriented fuzzy rule packages for torque

distribution operation while achieving fuel economy at the same time.

2. For the improvement of performance of IEMA, the sizes of driving data necessary for the operation of each subsystem in IEMA should be selected in an adaptive manner to cope with arbitrary driving situations.
3. The methodology to integrate the functioning of all subsystems should be addressed for increasing viability of IEMA.

Considering the above, the overall performance of the vehicle under the direction of IEMA would be better for driving in an arbitrary driving environment.

REFERENCES

- [1] D. Hermance and S. Sasaki, "Hybrid electric vehicles take to the streets," *IEEE Spectrum*, vol. 35, no. 11, pp. 48–52, November 1998.
- [2] V. Wouk, "Hybrids: Then and now," *IEEE Spectrum*, vol. 32, no. 7, pp. 16–21, July 1995.
- [3] M. Riezenman, "Engineering the EV future," *IEEE Spectrum*, vol. 35, no. 11, pp. 18–20, November 1998.
- [4] D. Buntin and J. W. Howze, "A switching logic controller for a hybrid electric/ICE vehicle," in *Proc. of the American Control Conf.*, vol. 2, Seattle, WA, June 1995, pp. 1169–1175.
- [5] N. Jalil, N. A. Kheir, and M. Salman, "A rule-based energy management strategy for a series hybrid vehicle," in *Proc. of the American Control Conf.*, vol. 1, Albuquerque, NM, June 1997, pp. 689–693.
- [6] C. Liang, W. Qingnian, L. Youde, M. Zhimin, Z. Ziliang, and L. Di, "Study of the electric control strategy for the power train of hybrid electric vehicle," in *Proc. of the IEEE International Vehicle Electronics Conf. (IVEC '99)*, vol. 1, Changchun, China, September 1999, pp. 383–386.
- [7] E. Cerruto, A. Consoli, A. Raciti, and A. Testa, "Energy flows management in hybrid vehicles by fuzzy logic controller," in *Proc., 7th Mediterranean Electrotechnical Conf.*, vol. 3, Antalya, Turkey, April 1994, pp. 1314–1317.
- [8] ———, "Fuzzy logic based efficiency improvement of an urban electric vehicle," in *20th International Conf. on Industrial Electronics, Control and Instrumentation (IECON '94)*, vol. 2, Bologna, Italy, September 1994, pp. 1304–1309.
- [9] S. D. Farrall and R. P. Jones, "Energy management in an automotive electric/heat engine hybrid powertrain using fuzzy decision making," in *Proc. of the 1993 IEEE International Symp. on Intelligent Control*, Chicago, IL, August 1993, pp. 463–468.
- [10] H.-D. Lee, E.-S. Koo, S.-K. Kim, and J.-S. Kim, "Torque control strategy for a parallel-hybrid vehicle using fuzzy logic," *IEEE Industry Applications Magazine*, vol. 6, no. 6, pp. 33–38, November/December 2000.
- [11] E.-S. Koo, H.-D. Lee, S.-K. Sul, and J.-S. Kim, "Torque control strategy for parallel hybrid vehicle using fuzzy logic," in *Proc. of the 33rd IEEE Industrial Applications Society Annual Meeting*, vol. 3, St. Louis, MO, October 1998, pp. 1715–1720.
- [12] A. Brahma, B. Glenn, B. Guezenec, T. Miller, G. Rizzoni, and G. Washigton, "Modeling, performance analysis and control design of a hybrid sport-utility vehicle," in *Proc. of the 1999 IEEE International Conf. on Control Applications*, Kohara Coast-Island of Hawaii, HI, August 1999, pp. 1715–1720.

- [13] M. Salman, N. J. Schouten, and N. A. Kheir, "Control strategies for parallel hybrid vehicles," in *Proc. of the American Control Conf.*, Chicago, IL, June 2000, pp. 524–528.
- [14] J.-S. Won and R. Langari, "Fuzzy torque distribution control for a parallel hybrid vehicle," *Expert Systems: The International Journal of Knowledge Engineering and Neural Networks*, vol. 19, no. 1, pp. 4–10, February 2002.
- [15] N. J. Schouten, M. Salman, and N. Kheir, "Fuzzy logic control for parallel hybrid vehicles," *IEEE Trans. on Cont. Syst. Technology*, vol. 10, no. 3, pp. 460–468, May 2002.
- [16] S. E. Lyshevski and C. Yokomoto, "Control of hybrid-electric vehicles," in *Proc. of the American Control Conf.*, Philadelphia, PA, June 1998, pp. 2148–2149.
- [17] S. Delprat, T. M. Guerra, and J. Rimaux, "Control strategies for hybrid vehicles: Optimal control," in *Proc., Vehicular Technology Conf. (VTC 2002-Fall)*, vol. 3, Vancouver, Canada, September 2002, pp. 1681–1685.
- [18] A. Kleimaier and D. Schröder, "Optimization strategy for design and control of a hybrid vehicle," in *Proc., 6th International Workshop on Advanced Motion Control*, Nagoya, Japan, March 30 - April 1 2000, pp. 459–464.
- [19] H. Mosbech, "Optimal control of hybrid vehicle," in *Proc., International Symp. on Automotive Technology & Automation (ISATA '80)*, vol. 2, Turin, Italy, September 1980, pp. 303–320.
- [20] M. Oprean, V. Ionescu, N. Mocanu, S. Beloiu, and C. Stanciu, "Dynamic programming applied to hybrid vehicle control," in *Proc. of the International Conf. on Electric Drives (ICED 88)*, vol. 4, Poiana BRA W SOV, Romania, September 1988, pp. D2/10/1–20.
- [21] A. Brahma, Y. Guezennec, and G. Rizzoni, "Optimal energy management in series hybrid electric vehicles," in *Proc. of the American Control Conf.*, Chicago, IL, June 2000, pp. 60–64.
- [22] J. Bumby and I. Forster, "Optimisation and control of a hybrid electric car," *IEE Proceedings*, vol. 134. Part D, no. 6, pp. 373–387, November 1987.
- [23] C. Kim, E. NamGoong, S. Lee, T. Kim, and H. Kim, "Fuel economy optimization for parallel hybrid vehicles with CVT," SAE Paper No. 1999-01-1148, 1999.
- [24] E. D. Tate and S. P. Boyd, "Finding ultimate limits of performance for hybrid electric vehicles," SAE Paper No. 2000-01-3099, 2000.
- [25] V. H. Johnson, K. B. Wipke, and D. J. Rausen, "HEV control strategy for real-time optimization of fuel economy and emissions," SAE Paper No. 2001-01-1543, 2000.
- [26] G. Paganelli, M. Tateno, A. Brahma, G. Rizzoni, and Y. Guezennec, "Control development for a hybrid-electric sport-utility vehicle: Strategy, implementation and test results," in *Proc. of the American Control Conf.*, vol. 6, Arlington, VA, June 2001, pp. 5064–5069.

- [27] J.-S. Won, R. Langari, and M. Ehsani, "Energy management strategy for a parallel hybrid vehicle," in *Proc. of International Mechanical Engineering Congress and Exposition (IMECE '02)*, New Orleans, LA, November 2002, pp. IMECE2002-33 460.
- [28] S.-I. Jeon, S.-T. Jo, Y.-I. Park, and J.-M. Lee, "Multi-mode driving control of a parallel hybrid electric vehicle using driving pattern recognition," *Journal of Dynamic Systems, Measurement, and Control*, vol. 124, pp. 141-149, March 2002.
- [29] T. C. Moore and A. B. Lovins, "Vehicle design strategies to meet and exceed PNGV goals," SAE Paper No. 951906, 1995.
- [30] R. Bata, Y. Yacoub, W. Wang, D. Lyons, M. Gambino, and G. Rideout, "Heavy duty testing cycles: Survey and comparison," SAE Paper No. 942263, 1994.
- [31] E. Ericsson, "Independent driving pattern factors and their influence on fuel-use and exhaust emission factors," *Transportation Research Part D*, vol. 6, pp. 325-341, 2001.
- [32] ———, "Variability in urban driving patterns," *Transportation Research Part D*, vol. 5, pp. 337-354, 2000.
- [33] J.-P. Crauser, M. Maurin, and R. Joumard, "Representative kinematic sequences for the road traffic in France," SAE Paper No. 890875, 1989.
- [34] M. Kuhler and D. Karstens, "Improved driving cycle for testing automotive exhaust emissions," SAE Paper No. 780650, 1978.
- [35] T. R. Carlson and R. C. Austin, "Development of speed correction cycles," Sierra Research, Inc., Sacramento, CA, Report SR97-04-01, April 30 1997.
- [36] *Highway Capacity Manual 2000*. Washington, DC: Transportation Research Board, 2000.
- [37] M. T. Hagan, H. B. Demuth, and M. Beale, *Neural Network Design*. Boston, MA: PWS Publishing Co., 1995.
- [38] W. R. McShane and R. P. Roess, *Traffic Engineering*. Englewood Cliffs, NJ: Prentice-Hall, 1990.
- [39] B. A. Holmén and D. A. Niemeier, "Characterizing the effects of driver variability on real-world vehicle emissions," *Transportation Research Part D*, vol. 3, pp. 117-128, 1997.
- [40] D. C. LeBlanc, F. M. Saunders, M. D. Meyer, and R. Guensler, "Driving pattern variability and impacts on vehicle carbon monoxide emissions," in *Transportation Research Record*. Transportation Research Board, National Research Council, 1995, no. 1472, pp. 45-52.
- [41] I. De Vlieger, D. De Keukeleere, and J. Kretzschmar, "Environmental effects of driving behaviors and congestion related to passenger cars," *Atmospheric Environment*, no. 34, pp. 4649-4655, 2000.

- [42] I. De Vlieger, "On-board emission and fuel consumption measurement campaign on petrol-driven passenger cars," *Atmospheric Environment*, vol. 3, no. 22, pp. 3753–3761, 1997.
- [43] —, "Influence of driving behavior on fuel consumption," in *Proc., ECODRIVE 7th Conference*, Graz, Austria, September 1997, p. 90, available at <http://www.ecodrive.at/english/index.html>.
- [44] L. Smith, "Reducing the environmental impact on driving-effectiveness of driver training," in *Proc., ECODRIVE 7th Conference*, Graz, Austria, September 1997, pp. 48–55, available at <http://www.ecodrive.at/english/index.html>.
- [45] T. Preben, "Positive side effects of an economical driving style: Safety, emissions, noise, costs," in *Proc., ECODRIVE 7th Conference*, Graz, Austria, September 1997, pp. 68–71, available at <http://www.ecodrive.at/english/index.html>.
- [46] StatSoft, Inc., *Electronic Statistics Textbook*, Tulsa, OK, 2002, available at <http://www.statsoft.com/textbook/stathome.html>.
- [47] J. Cloke, G. Harris, S. Latham, A. Quimby, E. Smith, and C. Baughan, "Reducing the environmental impact of driving: a review of training and in-vehicle technologies," Transport Research Laboratory, Crowthorne, Berkshire, Report 384, 1999.
- [48] Environmental Protection Agency, "Federal test procedure revisions (Web-page)," available at <http://www.epa.gov/otag/sftp.htm>.
- [49] D. L. Buntin, "Control system design for a parallel hybrid electric vehicle," M.S. Thesis, Texas A&M University, College Station, TX, August 1994.
- [50] T. C. Austion, T. R. Carlson, and R. G. Dulla, "Methodology for generating driving cycles for inventory development," Sierra Research, Inc., Sacramento, CA, Report SR95-09-02, September 29 1995.

APPENDIX A

DESCRIPTION OF DRIVING PATTERN PARAMETERS

Driving pattern parameters listed here is from Ericsson [31].

Trip time* : Total time of driving

Trip distance* : Total distance of driving.

v_avg : Average speed

v_std : Standard Deviation (SD) of speed

*v_max** : Maximum speed

a_avg : Average acceleration

a_std : SD of acceleration

*a_max** : Maximum acceleration

r_avg : Average deceleration

r_std : SD of deceleration

*r_max** : Maximum deceleration

mm_100m : Number of acceleration/deceleration shifts per 100 m where the difference between adjacent local max-speed and min-speed was > 2 km/h

lmm_100m : Number of acceleration/deceleration shifts per 100 m where the difference between adjacent local max-speed and min-speed was > 10 km/h

mm_100s : Number of acceleration/deceleration shifts per 100 s where the difference between adjacent local max-speed and min-speed was > 2 km/h

lmm_100s : Number of acceleration/deceleration shifts per 100 s where the difference between adjacent local max-speed and min-speed was > 10 km/h

RPA : Relative positive acceleration: $\frac{1}{x} \int va^+ dt$, $a^+ = \frac{dv}{dt}$, x = total distance

Int_a2 : Integral of the square of the acceleration: $\frac{1}{n} \int a^2 dt$, n = No. of time steps

pc.stopt : % of time when speed < 2 km/h

stop_dura : Average stop duration

stop_pkm : Number of stops per km

- n_stop^* : Number of stops
 v_{0-00}^* : % of time at speed 0 km/h
 v_{0-15} : % of time in speed interval 0 – 15 km/h
 v_{15-30} : % of time in speed interval 15 – 30 km/h
 v_{30-50} : % of time in speed interval 30 – 50 km/h
 v_{50-70} : % of time in speed interval 50 – 70 km/h
 v_{70-90} : % of time in speed interval 70 – 90 km/h
 v_{90-110} : % of time in speed interval 90 – 110 km/h
 $v_{110-200}$: % of time in speed interval > 110 km/h
 r_{100-25} : % of time in deceleration interval $-10 \sim -2.5$ m/s
 r_{25-15} : % of time in deceleration interval $-2.5 \sim -1.5$ m/s
 r_{15-10} : % of time in deceleration interval $-1.5 \sim -1.0$ m/s
 r_{10-05} : % of time in deceleration interval $-1.0 \sim -0.5$ m/s
 r_{05-0} : % of time in deceleration interval $-0.5 \sim 0$ m/s
 a_{0-05} : % of time in acceleration interval $0 \sim 0.5$ m/s
 a_{05-10} : % of time in acceleration interval $0.5 \sim 1.0$ m/s
 a_{10-15} : % of time in acceleration interval $1.0 \sim 1.5$ m/s
 a_{15-25} : % of time in acceleration interval $1.5 \sim 2.5$ m/s
 a_{25-100} : % of time in acceleration interval $2.5 \sim 10$ m/s
PKE : Positive kinetic energy, $PKE = \frac{\sum(v_f^2 - v_s^2)}{x}$, when $\frac{dv}{dt} > 0$, v_f =final speed, v_s =start speed, x =distance
 va_0 : % of time when $va < 0$ m²/s³
 va_{0-3} : % of time when va is $0 \sim 3$ m²/s³
 va_{3-6} : % of time when va is $3 \sim 6$ m²/s³
 va_{6-10} : % of time when va is $6 \sim 10$ m²/s³
 va_{10-15} : % of time when va is $10 \sim 15$ m²/s³
 va_{15-99} : % of time when va is > 15 m²/s³
 va_avg : Average va in m²/s³

The parameters with superscript * are additionally added to the list by the author.

VITA

Jong-Seob Won, the third son of Chang-Hee Won and Bok-Seon Bae, was born on December 5, 1964, in Pusan, Korea. He received a Bachelor of Science degree in Mechanical and Precision Engineering from Pusan National University, Korea in 1988. He was employed at the Agency for Defense Development in Korea as a research engineer, where he was involved in the project for the development of basic trainer aircraft from 1993 to 1996. He married So-Ra in 1996 and became a father of one son, Doo-Hyeon, in 1999. He received a Master of Science degree in Mechanical Engineering from Texas A&M University in College Station, Texas in 1998. He continued his studies in Mechanical Engineering under the direction of Associate Professor Reza Langari, and received a Doctor of Philosophy degree in Mechanical Engineering from Texas A&M University in May 2003. His permanent address is 7/1 260-7 Koijeong-3-Dong Saha-Ku, Pusan, KOREA, 604-083.